Imaging the Injured Lung: Mechanisms of Action and Clinical Use

Maurizio Cereda, MD[1], **Yi Xin, MS**[2], **Alberto Goffi, MD**[3], **Jacob Herrmann, MS**[4], **David W. Kaczka, MD PhD**[5], **Brian P. Kavanagh, MD**[6], **Gaetano Perchiazzi, MD PhD**[7], **Takeshi Yoshida, MD PhD**[6], **Rahim R. Rizi, PhD**[2]

[1]Department of Anesthesiology and Critical Care, University of Pennsylvania, Philadelphia, PA, USA;

[2]Department of Radiology, University of Pennsylvania, Philadelphia, PA, USA;

[3]Interdepartmental Division of Critical Care Medicine and Department of Medicine, University of Toronto, ON, Canada;

[4]Departments of Anesthesia and Biomedical Engineering, University of Iowa, IA;

[5]Departments of Anesthesia, Radiology, and Biomedical Engineering, University of Iowa, IA;

[6]Hospital for Sick Children, University of Toronto, ON, Canada;

[7]Hedenstierna Laboratory and Uppsala University Hospital, Uppsala University, Sweden.

Abstract

The Acute Respiratory Distress Syndrome (ARDS) consists of acute hypoxemic respiratory failure characterized by massive and heterogeneously distributed loss of lung aeration caused by diffuse inflammation and edema present in interstitial and alveolar spaces. It is defined by consensus criteria which include diffuse infiltrates on chest imaging - either plain radiography or computed tomography (CT). In this review we will summarize how imaging sciences can inform modern respiratory management of ARDS and continue to increase our understanding of the acutely injured lung. We describe also newer imaging methodologies that are likely to inform future clinical decision-making and potentially improve outcome. For each imaging modality we systematically describe the underlying principles, the technology involved, measurements obtained, insights gained by the technique, emerging approaches, limitations and future

CORRESPONDING AUTHOR: Maurizio Cereda, MD, Department of Anesthesiology and Critical Care, Perelman School of Medicine at the University of Pennsylvania, Dulles 773, 3400 Spruce Street Philadelphia, PA 19104-4283. Tel: (215) 300-1519. maurizio.cereda@uphs.upenn.edu.

developments. Finally, we consider integrated approaches whereby multimodal imaging may impact on management of ARDS.

EVOLUTION OF IMAGING IN ARDS

Plain chest radiography enabled the original description of ARDS,[1] and -*decades later*-computed tomography (CT) revealed that diffuse lung densities are in fact heterogeneously distributed.[2] In retrospect, this is easy to understand: plain radiographs provide a 2-dimensional image of the chest (Figure 1A), but except for classical pointers (*e.g.* silhouette sign), cannot reliably indicate where in the dorsal-ventral dimension the infiltrate is located; nor, can it differentiate among combinations of superimposed aerated, consolidated or atelectatic lung.[3] The most obvious advance provided by the CT scan was the identification, in patients managed in the supine position, of the massive loss of lung aeration predominating in dorsal regions whereas ventral regions remained partially or fully aerated and received the most part of tidal volume (Figure 1B).[2,4,5] This concept of the 'baby lung' enabled the 'spatial' rationale for tidal volume (V_T) limitation,[6,7] and provided important evidence for prone positioning for patients with ARDS,[8,9] as well as for the concept of recruiting non-aerated lung[5,10,11]

The idea of the 'baby lung' as the vulnerable region (receiving the bulk of each V_T) received support -decades later- from positron emission tomography (PET) demonstrating co-localization of ventilator-induced stretch in the 'baby lung' (CT) and ventral inflammation (PET), in proportion to the degree of stretch.[12,13] Using sophisticated CT imaging[14] with high spatial resolution,[15] recent studies suggest that the concept of the 'baby lung' can be further refined. Because the lung aeration in ARDS is inhomogeneous even at a far smaller scale -too small to be distinguished by CT - such that microscale regions surrounded by atelectatic lung may undergo disproportionate degrees of (unrecognized) stretch, analogous to the macroscale 'baby lung'.[16-18] This may mean that there are two 'levels' of 'baby lung', one macroscopic and mostly ventral, the other microscopic and diffuse, and different imaging would be necessary to visualize and manage each.

While plain radiography and CT contribute to patient care in ARDS,[3] risks of transport, radiation, and limitations of interpretation continue to be challenges. In addition, the complexity of image processing is an important obstacle.[19] Lung ultrasound (LUS) and electrical impedance tomography (EIT) increasingly allow serial assessment of the lung (and thorax) at the bedside, and are increasingly reported to assist in monitoring disease progression, response to intervention, and titration of ventilator settings.[20-26] However, challenges remain in terms of spatial resolution and tissue penetration.

Magnetic resonance imaging (MRI) had found limited use in acute respiratory medicine, but recent methodologies have advanced our knowledge of lung function[16,27-29] and metabolism.[30,31]

Overriding these developments is recognition of the inherent limitations of the current clinical criteria for ARDS.[32] Because these are based on oxygenation, end-expiratory pressure and the presence (*vs.* absence) of pulmonary infiltrates on plain radiography, it is

not possible to distinguish among several phenotypic[33] or physiological characteristics[34] that likely affect outcome and response to intervention.[35] Indeed, such variability confounds the results of most clinical trials[36] and complicates patient selection for complex or high-risk treatments, such as extracorporeal lung assist or stem cell therapy. A major opportunity for the field will be incorporation of lung imaging -together with emerging biologic techniques- to help characterize patients or groups of patients and thereby facilitate clinical discovery and management in ARDS onto a progressively more biological basis.[37]

CHEST RADIOGRAPH

The chest radiograph (CXR) has for decades been a cornerstone for diagnosis and management in acute medicine. All definitions to date [38,40] have included acute infiltrates on CXR as requirements for diagnosis of ARDS (Figure 1A). While newer imaging modalities are emerging into clinical practice, the traditional CXR has deep roots in the culture and practice of critical care.

Principles:

Plain chest x-ray yields a two-dimensional projection image, typically acquired from frontal and sometimes additional lateral views. There are two basic elements, an X-ray generator, and a detector. X-ray images display the contrast between organs based on the attenuation (*i.e.* absorption) of X-ray energy. For example, the lung mostly contains air and compared to the ribcage, has minimum attenuation of the x-ray beam. Loss of lung aeration caused by edema or infiltration in the lung is contrasted against healthy (*i.e.* air-filled) parenchyma.

Technology:

A standard chest radiograph delivers a radiation dose of approximately 0.1 mSv (comparable to the dose absorbed in a transoceanic flight). Because there are two (not three) dimensions, the absolute pixel value in x-ray cannot correspond to a specific tissue density, unlike the fixed scale in CT; for this reason, quantitative analysis of plain CXR is difficult. Radiologists instead use the relative contrast of images, and pattern recognition skills, to formulate diagnoses. Critically ill patients are imaged by portable machines, where the generator is at closer distance to the detector than in ambulatory radiography, and the x-ray beam originates anteriorly to the patient.

Measurements and Uses:

Chest x-ray is highly accessible; it is a standard in every ICU, and aside from diagnosis (presence of bilateral infiltrates, and absence of suggestion of a cardiac cause), it is used in the course of ARDS to complement clinical assessment and parameters for gas exchange and mechanics, to determine overall trajectory, in addition to the identification of intercurrent issues such as pleural effusion, atelectasis, pneumothorax, and correct placement of endotracheal tubes and central venous catheters.

Insights and Contributions:

Although the Berlin definition allows using CT in alternative, the CXR is an integral component of the ARDS criteria. [39] CXR has been used to grade ARDS severity,[40] and to

monitor disease progression and treatment responses. The description of bilateral infiltrates in ARDS has not changed significantly since the original publication; indeed, the authors described patchy infiltrates that were 'frequently confused with acute heart-failure'.[1] Opacities are initially hazy, mostly symmetric, and have ill-defined vascular margins that tend to disappear as the infiltrates become more confluent, leading to loss of diaphragmatic and cardiac margins.[41] Signs of fibrosis or extra-alveolar air (interstitial emphysema, pneumothorax) may appear with prolonged ventilation, especially with elevated V_T.

Emerging Developments:

The traditional X-ray is a century old imaging tool. Modern image acquisition has shifted from analogue films to fully digital. Contemporary images are instantly produced and available on the device seconds after the examination has been performed. Current x-ray systems are becoming more compact and portable, and are used in the ICU with minimum care disruption, and are almost always instantly digitized.

Challenges and Limitations:

Compared to the standard postero-anterior technique, portable CXR has technical limitations decreasing image quality. These include geometric distortion, scattered dose fraction, lower energy, presence of wires and tubes, and motion artifacts due to breathing.[42] Agreement on interpretation of CXR is surprisingly poor. CXR has limited accuracy (39-70% sensitivity and 70-100% specificity when using CT as reference) in detecting radiological abnormalities characteristic of ARDS.[42,43] While bilateral infiltrates on plain radiograph (Figure 1A) are required to diagnose ARDS,[39] it is often impossible to reliably differentiate among atelectasis, pleural fluid, consolidation, and hydrostatic or permeability edema.[3,44] In fact, bilateral infiltrates do not help accurately identify diffuse alveolar damage.[45-47] The agreement among experts as to the presence of pulmonary infiltrates (without regard to what the infiltrates represent) in patients being evaluated for ARDS, is low (kappa statistic for agreement is 0.38 - 0.55).[48,49] This has not improved (kappa = 0.50) with the more recent Berlin Definition[50] despite the radiographic criteria being more explicit ('bilateral opacities —not fully explained by effusions, lobar/lung collapse, or nodules), the availability of a set of example images,[32] and the adoption of a training program.[51]

Future Developments:

The diagnostic accuracy of plain radiography can be improved with the aid of semi-automatic algorithms,[52] becoming fully automated with machine learning and deep learning. [53] In 'deep learning' methodologies, computers are trained to recognize features directly from images in a fully automated manner. In a recent study, the trained deep learning algorithm outperformed practicing radiologists for the detection or pneumonia and other pathologies in chest x-ray images,[53] notwithstanding the fact that relevant patient information was not made available to the computer programs. Further improvements in artificial intelligence and deep learning algorithms will be possible with the availability of extensive data sets, including clinical information. To facilitate this progress, the National Institutes of Health has recently shared a new database (ChestX-ray14)[54] consisting of more than 100,000 images of more than 30,000 unique patients, together with the radiology reports. Furthermore, the limitations of computation cost and algorithm complexity will

almost certainly be easy to overcome over time. While these technological improvements are likely to augment the reliability of chest radiography, it is uncertain if the specificity (*e.g.* for lung inflammation or other biological processes) will be improved, and the limitations of 'consensus' ARDS definitions may persist.

COMPUTED TOMOGRAPHY

CT represents thoracic structures in three dimensions; it refines the morphological assessment of the lung aeration in ARDS, and combined with quantitative analysis of regional tissue density,[55] it powerfully measures the severity of lung injury. Recent image processing yields spatial resolution approaching the acinar level, and provides detailed maps of regional ventilation[56] and lung stretch.[57,58]

Principles:

CT provides three-dimensional representations of anatomic structures by reconstructing images of the same object obtained from multiple directions as the X-ray generator and the detector rotate. CT represents each element of tissue volume (*i.e.* each voxel) within the reconstructed image by quantifying its density according to attenuation of X-Ray energy in relation to typical values for air and water (Figure 2A). The spectrum of density is visualized with an arbitrary 'grey scale' that ranges from 'white' to 'black' and is adjusted by the radiologist.

Technology:

In a modern (multi-detector spiral CT) scanner, the x-ray generator and detector are rigidly fixed on opposite sides of the subject, rotating in the same direction (i.e., both clockwise or both counter-clockwise), creating a helical path around the subject. This substantially reduces acquisition time, motion artifacts, and radiation exposure (≈7 mSv for a high-resolution spiral thorax CT, compared with ≈ 0.1 mSv for a standard CXR and ≈ 12 mSv for CT pulmonary or coronary angiography).

Measurements and Uses:

CT has multiple uses in assessment, intervention, and research.

Diagnostic Use: Compared to plain radiography, CT is more accurate for the detection and localization of pleural effusion, pneumothorax, alveolar-interstitial syndrome, atelectasis, and lung consolidation.[59,60] While not necessary for a diagnosis of ARDS,[39] a 'ground glass' appearance on CT (Figure 1C; *i.e.* partial, but not abolished, aeration) is characteristic.[61] CT might improve the accuracy of ARDS diagnosis vs. CXR,[43] but correlation with pathological standard is unclear.

In the supine position, complete opacification of posterior and caudal lung regions is typical, due to alveolar atelectasis, infiltration and flooding. In ARDS, predominant non-dependent [62]opacities suggest lung superinfection, whereas in the absence of ARDS, 'tree-in-bud'[63] opacifications and/or consolidation of lower lobes[64] suggest community-acquired and ventilator-associated pneumonia

By contrast, predominant non-dependent[62] and 'tree-in bud'[63] opacifications suggest pneumonia (which can co-exist with ARDS), and important ARDS 'mimickers' such as interstitial lung disease or bronchiolitis obliterans with organizing pneumonia are readily distinguished.[65]

CT impacts clinical decision in over 20% of cases.[59,66] Chronic phases of ARDS are characterized by progressive fibrosis,[67] fibrotic reticulations, traction bronchiectasis (*i.e.*, bronchial dilatation generated by parenchymal loss), and cysts that evolve into a 'honeycomb' pattern.[61] In addition, bullous lesions and extra-pulmonary air reflect barotrauma and hyperinflation due to mechanical ventilation (Figure 1D).[67,68] Adverse prognosis is associated with greater proportions of abnormal tissue (*e.g.* consolidation, ground glass opacification)[69] and fibroproliferative changes.[70]

Quantitative Analysis: For quantitative analysis beyond routine interpretation, further image processing is needed, as follows: the lungs are segmented (from non-pulmonary structures), and the tissue densities averaged and analyzed within regions of interest, such as horizontal slices.[10] In ARDS, segmentation requires time and experience to distinguish high density parenchyma from effusion or chest wall; but, new algorithms automate this task.[71-73]

X-Ray attenuation (*i.e.* absorption) in each voxel is expressed in Hounsfield units (HU) after calibration against reference standards (*i.e.* density of water yields zero HU, and density of air is -1000 HU (Figure 2A). Assuming that completely non-aerated (degassed) lung tissue has density similar to water (0 HU), it can be stated that the density of each voxel reflects its relative proportions of gas *vs.* tissue.[74,75] Thus, normal lung tissue is -700 HU (corresponding to 70% air, 30% tissue).[76] Within the normal inflation range (-500 to -900 HU), higher HU values are more frequent at low lung volumes (*e.g.* functional residual capacity), and lower HU values are more common at higher volumes (*e.g.* approaching total lung capacity). Atelectasis, edema, and infiltrates have HU values close to zero, indicating absence of aeration; and, hyperinflated lung (emphysema, or ARDS during mechanical ventilation) is less than -900 HU.[77] Densities from -100 to -500 HU (*e.g.* ground glass) indicate decreased (but not abolished) gas content.[78]

Each voxel (≈ 1 mm^3) contains up to 170 alveoli[79] and therefore CT necessarily involves a degree of tissue averaging within each voxel, resulting in increased levels of intermediate density (-100 to -500 HU) when ventilated and non-ventilated airspaces are mixed (Figure 2B).

Functional CT: While lung structure and aeration are deduced from standard volumetric images, functional characteristics can be determined using specialized imaging protocols. Tidal variation in structure or aeration may be assessed between (pairs of) volumetric images that are acquired at end-expiratory and end-inspiratory breath-holds.[14] The deformation and motion of thoracic tissue between the image pairs may be estimated using three-dimensional image registration,[56,80-82] an image processing technique that aligns two or more images using the same spatial coordinates (Figure 3). Specialized registration functions for lung image processing [83,84] corrects for changes in tissue density changes associated with extremes of lung deformability (*e.g.* due to atelectasis). After registration, each matching

voxel can be tracked across aligned images when the shape of the entire lung changes due to inspiration, expiration or progression of injury (see also Supplemental Digital Content 1).

Acquisition of multiple volumetric images, characterizing thoracic motion throughout the breathing cycle, is possible using respiratory-gated image reconstruction, based on a surrogate lung volume signal or fixed respiratory rate. [81,84-86] As shown in Figure 4 and video Supplemental Digital Content 2, tidal recruitment results essentially from the transformation of poorly aerated into normally aerated lung regions and marginally from re-aeration of non-aerated lung regions. The same behavior is observed concerning PEEP-induced lung recruitment.[78] Four-dimensional image registration, estimating the motion of thoracic structures across space and breathing phase, expresses variation in regional lung strain and aeration, [87] as well as 'out-of-phase' lung motion. The accuracy of image registration was evaluated in an international challenge, although ARDS was not included.[88] However, image segmentation and registration remain complex tasks for automated processing,[89] especially in lung injury where consolidated or atelectatic lung limits structural reference points or contrast against the local chest wall.[56,71]

Regions of low ventilation may be identified using wash-in of a radiopaque tracer gas, such as xenon or krypton.[58,90-92] While image quality for tracer gas techniques is low, initial reports suggest that it may be enhanced by dual-energy CT.[92-95] Dual-energy CT relies on the contrast produced by sudden increases in photon absorption at specific energy levels - so-called 'K-edges', which denote the binding energy of K-shell electrons of atoms interacting with photons. Subtraction of images acquired using photon energies just above and below the 'K-edge' of a tracer gas provides a high-contrast image of gas distribution. [95-98]

Insights and Contributions:

CT has provided major insights into our understanding of ARDS, in the following areas.

Distribution of Inflation: In the supine position, hyperdensities predominate in dependent (dorsal) lung, while aerated tissue predominates in the non-dependent (ventral) lung.[2] It is possible to estimate the weight of each horizontal slab of tissue (product of the density multiplied by the tissue height) yielding the 'superimposed' pressure applied on each lung region[99,100] that contributes to the vertical gradient of pleural pressure.[101] This gradient is increased in lung injury and governs the distribution of regional density, supporting a model where dependent loss of aeration is explained, in part, by compression from overlying edematous lung,[100] mediastinum[102] and abdominal pressure,[5] in addition to the constrained shape-matching of the lung and the thorax.[103]

In ARDS, aerated lung is typically reduced to less than 50% of normal capacity[104] and this is mostly located in the ventral 'baby lung' -or as multiple smaller aerated areas scattered within the injured lung.[4] The 'baby' lung (Figure 1B) receives all the inhaled gas and tidal stretch in the 'baby lung' is therefore disproportionally large. Such hyperinflation in ventral lung[68] explains why this region is especially susceptible to ventilator induced injury; it also underscores why high V_T so readily causes lung injury, providing the rationale for current ventilator management of ARDS[6]

However, CT scans demonstrate that the size of the 'baby lung' is variable among patients with ARDS, thus a fixed low tidal volume may expose patients with very small lung capacity to overdistension;[105] conversely, it explains why very low VT could cause under-distension and atelectasis in those with very large lung capacity. Such insight has led to development of driving pressure instead of V_T as a potential ventilation target.[106,107]

Alveolar Recruitment: Recruiting poorly and non-aerated lung with PEEP or recruitment maneuvers increases aeration[10,99,108] and this can be expressed as *decrease* in weight of non-aerated lung[109] or, as increase in gas content within poorly and non-aerated lung regions.[78] CT studies show that lung reaerated during inflation might not remain aerated during expiration unless adequate PEEP is provided (Figure 5).[110] This is clinically important given the experimental evidence that unstable recruitment causes substantial intrapulmonary shunt[111] and may worsen ventilator-induced injury.[112] Furthermore, patients with ARDS who have massive loss of aeration (on CT) have higher mortality,[109] making loss of aeration either a marker of severity or a treatable factor. However, globally applied strategies to maintain lungs aerated have not increased survival.[113] This could be related to the fact that patients with focal vs. non-focal loss of aeration do not respond to recruitment maneuvers.[114]

Prone Positioning: In the supine position, the vertical gradients of pleural pressure are such that higher airway pressure (*e.g.* PEEP), preferentially distributes gas to the non-dependent (rather than the dependent) lung, causing preferential non-dependent hyperinflation rather than dorsal recruitment. This was noticed using plain radiography and led to the hypothesis that prone positioning favors more homogeneous aeration by decreasing the vertical pleural pressure gradient.[8] Later, studies using CT confirmed that the vertical gradient of CT density (superimposed pressure) is attenuated when prone[9] and that this lessens atelectasis, consolidation, cyclic derecruitment, and hyperinflation[115,116] which together may explain the lower mortality associated with prone positioning in ARDS.[117]

Imaging Phenotypes: Some patients share similar radiological appearance, treatment responses, or biological characteristics.[35,114,118] For example, the prominence of symmetric ground glass instead of focal opacification[119] suggests a non-pulmonary cause, reflecting blood-borne mediation of inflammation. In contrast, non-focal density distribution *vs.* prominent dependent loss of aeration suggests a favorable response to PEEP,[120] higher mortality,[121] and increased levels of circulating marker of alveolar cell injury such as soluble form of the receptor for advanced glycation end product (sRAGE).[118] Such features point to a high-severity phenotype with widespread pulmonary edema.[109] With this rationale, the recently concluded 'LIVE' (lung imaging morphology for ventilator settings in acute respiratory distress syndrome) tested the hypothesis that an imaging-guided ventilator strategy (targeting the different phenotypes) improves outcomes compared to a conventional (standardized) approach.[122]

Intratidal Variations: Measurements of pressure and flow at the airway opening have been associated with distributed mechanical phenomena throughout the lungs, including nonlinear deflections in the dynamic pressure-volume curve associated with recruitment and

overdistension.[123-126] However CT imaging at end-expiration and end-inspiration revealed intratidal variations in recruitment and overdistension that conflicted with predictions from pressure-volume data in injured lungs (despite there being good agreement under healthy conditions).[127] Instead, minimizing dynamic compliance in injured lungs by PEEP titration was found to be associated with reductions in both overdistension and intratidal recruitment. These findings highlight the value of medical imaging for heterogeneous lung injury, and indicate that dynamic mechanical alterations in the lung are difficult to quantify using only aggregate pressure-volume data, especially where recruitment and overdistension coexist.[128,129]

Emerging Developments:

Measuring regional lung function at very high resolution (*i.e.* subsegmental, acinar, alveolar) enables more accurate biological characterization. Injured lung inflates non-uniformly; while this can cause highly localized extremes of mechanical stress,[17] it can only be visualized with high spatial resolution. Computational calculation indicates greatest inhomogeneity surrounding each voxel at interfaces between aerated and non-aerated tissue, and at anatomical structures ('stress raisers').[130] Preliminary reports of this method in patients with ARDS suggests that the extent of 'stress raisers' reflects severity of injury.[15]

Photon counting CT produces an image based on unique spectral signatures,[131] yet relies on only a single X-ray source and specialized detectors capable of distinguishing among individual photons whereas conventional detectors integrate all photon energies. Photon counting may therefore enable contrast-based functional imaging similar to dual-energy CT, while involving reduced radiation exposure as well as enhanced ability to distinguish multiple contrast agents simultaneously.

ARDS results from the propagation of lung inflammation, initially localized (to one or more areas) then generalized. CT images suggest that this propagation may be driven or amplified by inspiratory stretch (see video, Supplemental Digital Content 3).[132] Image analysis using parametric response maps (PRM) can analyze inflation with voxel-by-voxel precision.[133] PRMs are plots of density distribution obtained from co-registered inspiratory and expiratory CT images (Figure 6 A, B). A pattern of suboptimal aeration and large tidal density swings (termed 'unstable inflation') is associated with increased propagation of experimental injury;[14] this was attenuated by prone positioning,[134] and unstable inflation may predict mortality in patients with ARDS (Figure 6 C, D).[14] Thus, unstable inflation may be a treatable target in ARDS.

Lung Perfusion: The coupling between ventilation and perfusion in response to regional oxygenation tension is closely regulated by a variety of mechanisms.[135] In ARDS, regional perfusion may be highly variable,[136] and impaired hypoxic pulmonary vasoconstriction (HPV) may worsen hypoxia because of increased shunt and ventilation-to-perfusion mismatch. While there are several techniques that may quantify regional perfusion using CT,[137] few are applied clinically. Most clinical measurements of CT perfusion are limited to detecting large defects (*e.g.* pulmonary emboli) or substantial enhancement (*e.g.* malignancies).[137]

Regional perfusion may be determined by a sequence of cardiac-gated images acquired during intravenous infusion of an iodinated contrast agent.[138,139] Following lung segmentation, CT images of the parenchyma can be partitioned into tissue and blood components. Using such a technique, Dakin *et al.* demonstrated that during ARDS, a greater proportion of blood flow is directed toward less aerated regions of the lung,[138] and the amount of blood flow to consolidated lung is correlated with the severity of hypoxemia. It is uncertain however, whether such physiological correlates of perfusion and hypoxemia are present in human ARDS,[140,141] or whether such measurements of blood flow in ARDS can aid the titration of mechanical ventilation.[138]

Challenges and Limitations:

CT densitometry provides averages for gas or tissue content in each voxel. In human scanners, the dimensions (*i.e.* spatial resolution) of each voxel is ≈ 1 mm^3, and CT cannot differentiate among different alveolar units within each voxel (Figure 2B). Radiation exposure and dose accumulation limit its use, and but doses can be reduced to ≈ 1 mSv while allowing accurate analysis.[142] Furthermore, interpolation allows whole lung quantitation from a limited set of CT slices.[143] Finally, while transport of critically ill patients to a scanner is problematic,[144] portable scanners are becoming more readily available.

Future Developments:

Quantitative CT analysis will reveal mechanisms of injury and treatment responses, but clinical assessment currently relies on subjective interpretation. Quantitative CT lacks a standard reference for clinical use, and post-image processing is complex, non-uniform, and time consuming. Rapidly evolving computational techniques are streamlining such processing, and deep learning -after model training- involves minimal time or computational resource. If supported by clinical trials, these approaches alone, or together with biomarkers, will improve management, risk stratification and trial selection for patients with ARDS.

POSITRON EMISSION TOMOGRAPHY

Positron Emission Tomography (PET) is a form of functional imaging that allows visualization of a physiological or pathological process by marking with radioactive isotopes, one (or more) of the substances involved in its pathways.

Principles:

PET employs atoms in which a proton is converted into a neutron (by spontaneously losing a positron, a positive beta particle, β+) and an electron neutrino; the chemical element changes to one with a lower atomic number and increased nuclear energetic stability. The biological molecule containing the radionuclide is introduced into the body and concentrates according to biochemical avidity of individual tissues and cells. After positrons are emitted from the tracer, they rapidly interact with electrons belonging to the local tissue, causing an 'annihilation' that produces two photons travelling in opposite directions (Figure 7). [145] The PET scanner contains a ring of detectors surrounding the structure of interest and the simultaneous detection of the two photons in opposite parts of the ring represents a true signal ('true coincidence'). To define the location of the emitting region, the PET software

notes the time frame of the photons' arrival in the detector, and the angle between their trajectories. The quality of the image is directly proportional to the time-resolution of the detector.

Technology:

A PET scanner is a large a ring-shaped structure that contains the positron detectors, through which the patients moves as in a CT scanner (they are often combined). Recently, smaller and portable devices have been developed but are limited to specific areas of the body[146] or for veterinarian use.[147] The cost of a PET scan largely depends on the cost of the tracer and the length of the exam (can follow a metabolic pathway for several hours). For example, a 2-hour lung exam using the radiolabeled glucose analog 2-[fluorine-18]-fluoro-2-deoxy-D-glucose ([^{18}F]-FDG) costs ≈ €1500 (plus personnel), and the cost-effectiveness depends on the pathology and the tracer. A ^{18}F-FDG PET exam delivers ≈14.0 mSv,[148] and more if combined with a CT scan.

Measurements & Uses:

Any biological pathway can be assessed by PET provided a positron-emitting version of a core pathway molecule can be administered. Many tracers have been used and more are being identified.[149,150] In studying lung injury, studies focusing on ventilation use inhaled or injected [^{13}N]-N_2; on perfusion, use injected [^{13}N]-N_2 or [^{15}O]-H_2O; and, on lung cell metabolic activity use [^{18}F]-FDG. More than one tracer can be used simultaneously.

Insights & Contributions:

Inhaled nitrogen as [^{13}N]-N_2 has been studied in experimental lung injury and interrupted at steady state inhalation; emission images obtained during tracer washout[151] delineated aerated lung volume and alveolar recruitment; in addition, aerated lung volume reflected closely traditional pressure-volume analysis. This approach was also used to determine regional specific lung volume change (V_T divided by the end-expiratory gas volume, but per region) which approximated to the regional specific ventilation estimated by [^{13}N]-N_2 washout.[152] When it is not possible to use a combined CT-PET scanner to identify the lung border (inhaled [^{13}N]-N_2 is distributed only in ventilated lung regions), then the simultaneous injection of [^{15}O]-H_2O (which has an intravascular distribution) will map the organ.

Intravenous injection of dissolved [^{13}N]-N_2 gas (in a saline solution) has yielded key insights[153-155] and provides regional information about perfusion, ventilation and shunt. After injection it will immediately reach a peak PET activity in the pulmonary circulation, which during apnea lowers to a plateau due to redistribution in the circulation. After the plateau, the washout curve during ventilation gives information on the level of alveolar ventilation. By this technique it has been possible to demonstrate that sustained inflation can displace perfusion from aerated regions towards non-aerated lung, and temporarily increase intrapulmonary shunt.[156]

The use of the glucose-analog [^{18}F]-FDG permits assessment of the metabolic activity of cells employing a glycolytic pathway.[157] As with glucose, [^{18}F]-FDG is transported into

cells and is phosphorylated. The [18F]-FDG, which cannot progress through the Krebs cycle, is trapped in the cells in which de-phosphorylation activity is low. As analogue of the glucose, the [18F]-FDG tracer has been extensively used for tissues relying on glucose metabolism, such as brain and tumors.

Neutrophil activation is heightened in ARDS[158] and increased PMN energy production and glucose consumption is prominent.[159] The neutrophil activity can be monitored using PET with [18F]-FDG, as neutrophils are largely responsible for its uptake, although persistence of a [18F]-FDG signal in neutrophil-depletion suggests that other cells play a role.[160]

The number of counts in the PET signal during [18F]-FDG administration aggregates the total number of neutrophils and their metabolic avidity for glucose. The quantification was initially developed for solid organs or tumors, and its use in (aerated) lung tissue may be subject to flaws. The Standardized Uptake Value (SUV) measures the [18F]-FDG uptake in a region of interest, corrected for the injected dose and a distribution parameter.[161] Although the SUV incorporates the [18F]-FDG signal from blood and tissue, lung physiopathology involves more complex kinetics including experimental data fitting within multi-compartmental models, and timed blood sampling while the PET scanner acquires positron counts.[162]

Lung tissue simultaneously contains different tissue densities and it may be necessary to discriminate between uptake per unit tissue, and the effects of dense (*e.g.* atelectasis) tissue or regional hypoventilation; this may be mitigated by a correction for lung density[163,164] or the inclusion of a 3-compartment (*i.e.* blood, tissue-precursor, tissue-metabolic) model[165,166] allowing separation of pre-phosphorylation from irreversible trapping of [18F]-FDG in the tissues. However, lung edema has a density that is close to that of tissue, and this further complicates such analysis.[167]

Identifying the location of inflammation during lung injury makes the [18F]-FDG PET an invaluable research tool with potential impact on the care of patients. For example, it is now clear that in patients with ARDS active inflammation during mechanical ventilation (without spontaneous effort) is localized to the non-dependent 'baby lung' in short-term observations[12,168] (Figure 8A) and this is supported by longer-term experiments.[13] These data confirmed older work demonstrating the same distribution of inflammation using localized biopsy,[169] further supporting low tidal volume ventilation to protect the 'baby lung'. In contrast, PET scan (in experimental animals) has revealed that the locus of injury during spontaneous effort appears to be in the dependent lung close to the diaphragm (Figure 8B).[170]

Recently, [18F]-FDG PET was used to study the relationship between a clinically relevant ventilator strategy and lung local neutrophil activity in an animal model of endotoxemia.[171] At 24h, [18F]-FDG uptake was increased to a greater extent in consolidated and moderate-high aeration regions than in normally aerated regions. Regional strain and pulmonary blood volume were both increased in high-phosphorylation area. The approach raised the possibility that inflammation is induced not only by the mechanical ventilator stretch, but that the interaction of ventilator strain with local blood flow, by maximizing microvascular

stress and the endothelial surface exposed to circulating inflammatory cells, could initiate or propagate injury. These concepts, supported also by recent animal studies, [172,173] suggest that the prevention of lung injury might involve careful management of hemodynamics, as well as ventilator management.

Challenges & Limitations:

The principal limitations for clinical use of PET are cost and duration of the exam, and the exposure to radiation from the chosen tracer. A typical lung PET exam cannot be performed at bedside, and transport of critically ill patients remains a barrier.

Future Developments:

Biomedical development of PET involves new hardware and analytic algorithms, as well as engineering of new tracers. In principle, a greater space and time resolution, together with improved scanner sensitivity, may improve image quality. Application in oncology has advanced the search for new tracers, and with this, the ability to image almost any biological process seems likely in the near future.[149]

MAGNETIC RESONANCE IMAGING

Magnetic Resonance Imaging (MRI) of soft tissue structures has revolutionized how physicians view the structure of the musculature, skeletal system, and brain. This technique offers superb contrast between tissue textures, as well as flexible acquisition with a variety of pulse sequences that can highlight specific targets (*e.g.* pathology, hemorrhage, nodules etc.). However, proton imaging of the lung is challenging due to the low tissue density and magnetic effects at air/tissue interfaces. Additionally, because patients can hold their breath for limited time, the requirement for prolonged immobility is often impractical. In recent years, however, improvements in proton image acquisition and development of hyperpolarized MRI are raising the prospects for MRI in the study of lung injury, with potential impact on clinical management of ARDS.

Principles:

MRI measures signals that are generated by the rotation of nuclei immersed in a strong magnetic field. To obtain images, nuclei are excited by external radiofrequency energy (illustrated in Figure 9), and the signal is then captured while the nuclei recover their original state. This is characterized by two time constants: T1 is the time constant with which the nuclei return to equilibrium; T2 is the transverse relaxation time, required for the nuclei to go out of phase with each other. Water and inflamed tissue appear bright in T2 weighted images because they have longer T2.MRI signal strength is function of the difference (polarization) between the number of spins aligned with the magnetic field and those aligned in the opposite direction. This fractional difference is minimal, yet signal is high in solid tissue because proton density is very high. To increase signal in the lungs, where protons are less abundant, nuclei such as helium-3 (^{3}He), xenon-129 (^{129}Xe), and carbon-13 (^{13}C), are hyperpolarized (*i.e.* aligned with the magnetic field) and delivered to the subject in gaseous or liquid form.

Technology:

Several technological advances are making MRI appropriate for lung imaging.

Hyperpolarized gas imaging.—Hyperpolarization is produced by transferring the angular momentum of a beam of circularly polarized (laser) light on to the spins of tracer nuclei (*i.e.* [3]He or [129]Xe).[174-177] Polarization rates of 30-50% are commonly achieved [178] and maintained for the time required for imaging. The hyperpolarized nuclei are delivered in a 20-79% concentration with the inspired gas, thus the inspired O_2 level is adequate for respiration. A very large signal enhancement relative to proton MRI is achieved (see video, Supplemental Digital Content 4 showing hyperpolarized gas imaging of healthy lungs during progressive inflation). In addition to measuring tracer density, radiofrequency pulses and magnetic gradients are delivered to study specific lung functions.

Hyperpolarized Liquid MRI.—MRI investigation of molecules such as ^{13}C pyruvate allows the study of metabolic flux in tissues, thanks to the ability of MR spectroscopy to distinguish molecular transformations. Due to low natural abundance and small nuclear spin of ^{13}C, the signal must be increased through processes of nuclear polarization.[179] The hyperpolarized molecule is then intravenously injected and downstream metabolites (e.g. lactate and alanine from hyperpolarized pyruvate) are regionally measured.

Measurements and Uses:

Proton MRI.—The edema and atelectasis present in inflamed lung tissue increase spin density and this facilitates image acquisition in the lungs. Proton MRI can thus be used to visualize atelectasis[180] and inflammatory changes.[181, 182] In addition, oxygen enhanced MRI exploits the enhancement by alveolar oxygen of proton signal. These phenomena have been exploited to study lung perfusion and ventilation in preliminary human studies.[183,184]

Hyperpolarized Gas MRI.—After delivery to the alveoli, inhaled nuclei of [3]He or [129]Xe are excited with pulse sequences designed to map alveolar mechanics,[185] partial pressures of oxygen,[186] or with Xe[129], capillary blood and tissue gas uptake.[28] The effects of disease and mechanical ventilation on alveolar mechanics are studied through application of diffusion-sensitizing gradients, yielding a value for the so-called apparent diffusion coefficient (ADC) for each voxel. The ADC measures the restriction imposed by the alveolar walls on the diffusion of inhaled tracer nuclei (Figure 10A) and lower values indicate smaller dimensions of intra-acinar airspace (*i.e.* the alveoli and the alveolar ducts).[187] Helium is well suited for this purpose because its small nucleus diffuses rapidly, allowing more for more detailed characterization of the spaces.[188] In addition to ADC, regional ventilation can be mapped by measuring voxel-wise signal build-up during consecutive hyperpolarized breaths.[189]

Insights and Contributions:

Hyperpolarized gas MRI interrogates microscopic structures that are far smaller than the imaged voxels.[187] This is because the ADC signal reflects the predominant dimensions of airspaces contained in each tissue unit, but without direct visualization. The information provided is complementary to CT, overcoming the limitations of spatial resolution and of tissue averaging. This was appreciated where healthy and injured lungs were ventilated

under conditions of suboptimal recruitment.[16,27] Hyperpolarized gas cannot reach non-ventilated alveoli and thus no signal is obtained (Figure 10B);[190] however, atelectasis causes inspired gas to concentrate in adjacent residual ventilated airspaces (Figure 10B), augmenting the ADC signal. Indeed, after surfactant depletion, ADC values were elevated (Figure 10C).[16,191] By contrast, CT typically displayed intermediate grayscale images (Figure 10B). The high values of ADC likely reflected overdistended airspaces in which ventilated and atelectatic alveoli are intermingled (Figure 10B). Thus, the data support a model whereby atelectasis is closely associated with airspace overdistension;[192] and, recruitment therefore decreased ADC.[16] Regional ventilation was also high in poorly recruited regions.[193] These studies suggest that in lung tissue with mixed inflation, airspaces may undergo dynamic stretch during ventilation, which could explain why mixed inflation is associated with progression of lung injury[14,134] and tissue inflammation.[13]

Emerging Developments:

Imaging hyperpolarized ^{13}C-pyruvate allows estimation of the impact of disease[31] and treatment[30] on metabolic flux in lung tissue. Quantities of lactate, pyruvate, and other metabolic byproducts are mapped as the carbon spectrum shifts with each chemical reaction. In rodent studies following acid aspiration, carbon MRI showed progressive increases in tissue lactate/pyruvate ratio, which were contained by lung recruitment.[30] With the ability to study an array of metabolites, this methodology could be a viable alternative to PET in the *in vivo* study of regional lung metabolism.

Hyperpolarized [129]Xe dissolves in tissue and therefore permits imaging of transfer across the alveolar-capillary barrier. Reflected in the spectral shift, xenon is then measured in the blood and in the interstitial space, in addition to the intra-alveolar phase. This behavior permits estimates of interstitial edema and hyperemia due to inflammation.[29,194] Thus, hyperpolarized [129]Xe MRI has the potential to track regional alterations of gas transfer and uptake in injured lungs.

Hyperpolarized MRI has advantages including shorter acquisition times and higher spatial resolution (than PET), as well as the lack of radiation exposure; and, increased rapidity of execution allows multiple acquisitions and therefore longitudinal analysis in a given imaging session.

Challenges and Limitations:

The use of MRI in critically ill patients raises safety issues due to prolonged time spent in the scanner, and the need for MR compatible (*i.e.* non-ferrous) monitoring and ventilation equipment.

Future Developments:

Hyperpolarized MRI is likely to become a clinical reality in the characterization of lung pathology, enhancing understanding of lung injury. In ARDS, combining modalities offers a unique opportunity to perform simultaneous, spatially correlated measurements of lung function and metabolism that are otherwise impossible in vivo.

ELECTRICAL IMPEDANCE TOMOGRAPHY

Electrical impedance tomography (EIT) is a non-invasive, bedside monitoring system that uses micro-electric current to monitor the distribution of tidal ventilation; the data are usually presented at the bedside as a continuous illustration in the sagittal plane.

Principles:

EIT injects micro-currents (high frequency, low amplitude) using 16 or 32 electrodes placed in a transverse (sagittal) plane around the thorax in order to obtain a cross-sectional image of lungs as 7-10 cm lung slice.[22,23] Pairs of electrodes inject current while the remaining electrodes read the resultant voltages generated by current passing through the thorax; the 'sensed' current varies according to the diameter of the chest wall and change in electrical conductivity (Figure 11A). This cycle is repeated using alternating electrodes and results in sets of 'raw' (unprocessed) EIT images; the devices can produce 50 images per second (*i.e.*, high time resolution: 0.02 sec), and image reconstruction generates raw EIT images from the measured voltages through the electrode plane.[22] Local changes in impedance are plotted in a matrix containing 860 (from a total of 1024; 32×32) pixels, and the reconstructed images represent relative impedance changes for each pixel (termed: delta Z; ΔZ or change in impedance), which is compared to a reference value for Z taken at the beginning of the data acquisition.

Most impedance changes (*i.e.* ΔZ) in the thorax are caused by an increase or decrease in intrapulmonary gas volume (*i.e.* V_T), and because of this, EIT is an appropriate tool to map the distribution of ventilation. Regional values of ΔZ have been shown to be proportional to changes in regional tissue aeration (gas content) as measured by CT images in the same cross-sectional planes,[195] where greater increase in volume (gas content) corresponds to higher impedance. Thus, the distribution of tidal ΔZ represents regional ventilation during each breath.

Technology:

EIT electrodes are imbedded in a distensible belt that is placed on the thorax, usually over the 5-6th intercostal space. Placement of the electrodes at more caudal levels risks encroachment of the diaphragm into the measurement plane during expiration.[22] The presence of major spinal or chest wall wounds, multiple chest tubes, non-conductive bandages, conductive wire sutures will interfere with current transmission, and distort the ΔZ; in addition, the EIT currents can potentially interfere with cardiac pacemaker or defibrillator function [22].

Measurements and Uses:

The key advantage of EIT is the ability to detect real-time information regional ventilation at the bedside; such information cannot be obtained by global monitoring (*e.g.* airway pressure, flow monitoring or blood gas measurement). Thus, EIT monitoring is important especially when lung is injured, and distribution of aeration becomes inhomogeneous.

EIT images measure the relative impedance changes (Z) for each pixel and this represents the regional tidal volume during each breath, and because the 'time resolution' is high (0.02 sec), it smoothly tracks the dynamic pattern of regional inflation and deflation (see video, Supplemental Digital Content 5), *i.e.*, the spatial distribution of ventilation at the bedside.

In order to quantify the regional distribution of ventilation, arbitrary so-called 'regions of interest' (ROI), such as quadrants or layers are described.[22] Analysis of EIT images based on ROIs is helpful to detect spatial heterogeneity. The most frequently used measurement is the ratio of ventral to dorsal ventilation. For patients with ARDS, this dimension is especially important because most of patients are ventilated in the supine position. For example, clinicians may suspect dorsal atelectasis or consolidation if EIT indicates predominantly ventral (*vs.* dorsal) distribution of ventilation (Figure 11B).

A specific metric of distribution of ventilation is the 'center of ventilation' (COV); this is an index to quantify shifts in regional tidal ventilation along the ventro-dorsal dimension. The range across which ventilation occurs is considered from 0% (all ventral) to 100% (all dorsal), such that perfectly homogeneous ventilation is represented as the bulk of the imaged ventilation at the axis mid-point (*i.e.* a 50% center of ventilation; Figure 11B).[196-198]

Finally, The amount of lung overinflation and collapse can be estimated by EIT at the bedside by the number of pixel units in which compliance changed before and after passing the best pixel compliance, while PEEP is progressively lowered in decremental steps.[24]

Insights and Contributions:

One contribution from the use of EIT has been the identification of a novel mechanism of effort-dependent lung injury. EIT revealed that vigorous spontaneous effort draws gas from the non-dependent lung (called Pendelluft), or from the trachea and ventilator, towards the dependent lung. This causes a transient, early inspiratory local over-distension and tidal recruitment in the dependent lung during early inspiration, corresponding, in space and time, to maximal intensity of the diaphragm contraction.[199] This is consistent with the finding that the bulk of effort-dependent lung injury occurs in dependent lung, the same region where strong effort causes a local over-distension and tidal recruitment.[170] In contrast, positive-pressure ventilation during muscle paralysis worsens lung injury in the non-dependent lung, *i.e.* the regions that typically receive most of the V_T.[169,200] Taken together, the emerging picture is that in ventilator-induced lung injury, either from vigorous effort or only positive-pressure, the injury occurs in the lung regions receiving the most stretch (or ventilation). In this sense, EIT has a substantial potential to identify regional vulnerability to injury and to guide important clinical choices, such as muscle relaxation to suppress diaphragm activity.[201]

Challenges and Limitations:

There are several limitations of the technique. *First*, although temporal resolution is excellent, spatial resolution is less than with CT.[22,24] *Second*, because EIT measures *relative* change in impedance, it cannot identify regions of abnormality in which tidal impedance changes do not occur (*e.g.*, preexisting atelectasis, pleural effusion, large bullae).[22,23] In the same way, EIT cannot identify the anatomical border between lung and non-pulmonary

tissues. *Third*, while EIT is a useful research tool and has immense potential to personalize ventilator strategy at bedside, there is as yet no proven outcome benefit with its use. *Finally*, much of the analysis is performed off-line which may limit immediate implementation of the results.

Future Developments:

Emerging approaches will likely have important patient relevance, *e.g.*, detection of tidal recruitment, pneumothorax, calculation of ventilation/perfusion ratio and estimation of cardiac output.[22,23]

LUNG ULTRASOUND

Lung ultrasound (LUS) is a useful diagnostic tool that can be applied in real time at the bedside.[20,202] It is an accurate and reproducible technique for the diagnosis and monitoring of many pulmonary and pleural conditions seen in critically ill patients.

Principles:

In ultrasound technology, piezoelectric materials generate high-frequency (MHz; *i.e.*, millions of cycles/sec) sound waves that travel through biologic tissues in a straight direction until they encounter boundaries between two tissues with different acoustic characteristics (*i.e.*, acoustic impedance). At these boundaries, a portion of the ultrasound energy is reflected back to the transducer, while the remainder continues until another boundary of different acoustic impedance is reached or the ultrasound energy is completely absorbed by the tissues.[20,203-205]

Sonographic images are generated on two key principles: travel time and intensity of reflection. An ultrasound wave travels from the transducer to a reflector and back to the transducer, in order to generate an image; the total elapsed time is called 'time of flight' and is directly related to the distance (*i.e.* depth) travelled. The brightness of the generated image is proportional to the intensity of reflection that occurs at a tissue interface, with weaker reflections appearing as darker (gray) pixels and stronger reflections as white pixels. Areas that do not reflect ultrasound (*i.e.*, no difference in acoustic impedance) appear as black. [20,203-205]

Distinctive interactions of ultrasound waves with tissues, physical properties of the ultrasound beam and specific image reconstruction algorithms, may generate erroneous images called artifacts, that impact image quality and interpretation.[203,205,206] Most ultrasound modalities, as echocardiography, vascular or abdominal ultrasound, aim to avoid such artifacts. However, in LUS, the distinctive characteristics of aerated lung tissue produce artifacts that provide useful information; thus, LUS requires understanding and systematic analysis of both artifactual and anatomical images.[20,26]

In normally aerated lungs, ultrasound waves are almost completely reflected at the interface between the pleura and the aerated lung, generating a hyperechoic (*i.e.*, bright) horizontal stripe, called the 'pleural line' (Figure 12A). Deep to this, multiple regularly spaced reverberation artifacts are seen, called 'A lines', and focal lung densities at the level of the

pleural line (*i.e.*, interlobular septa, micro-atelectasis) are also seen as short bright vertical artifacts (formerly called 'Z lines').[207,208] Finally, lung movements from breathing or transmission of cardiac contractions result in 'lung sliding' and 'lung pulse', respectively.[26]

Loss of aerated lung due to increased tissue content (*e.g.*, edema, consolidation) or atelectasis impacts transmission in specific patterns.[20,26,208] Partially de-aerated lung is heterogeneous, and this results in penetration through (more dense) or reflection from (less dense) lung areas.[209] The resulting hyperechoic 'B-lines' arise from the pleural line, extend through the screen without fading, and move in conjunctions with tidal lung movements. [26,210,211] The severity of aeration loss is thus assessed according to consensus recomendations[26]. Aeration is normal if only A-lines or fewer than three B-lines are present. Three or more B-lines in an intercostal space represent a region of decreased lung aeration (interstitial syndrome): B1-pattern is characterized by spaced B-lines and denotes moderate loss of lung aeration; B2-pattern demonstrates coalescent B-lines and is seen in severe loss of lung aeration (Figure 12B). The term 'consolidation' denotes absence of alveolar air associated with ultrasound propagation and 'within lung' reflection, generating anatomical tissue-like images (Figure 12C).[20,26,212] See also video, Supplemental Digital Content 6.

Technology:

The most important component of an ultrasound system is the transducer; this contains the piezoelectric material converting electrical to mechanical (ultrasound) energy, and *vice versa*. The type of transducer impacts image interpretation,[213] and is chosen depending on the lung region and the clinical question (Table 1).[214] Two main features characterize different transducers: shape of the footprint and frequency of ultrasound waves. Larger footprints (*e.g.*, curvilinear) allow for broader scanning areas, whereas smaller footprints (*e.g.*, microconvex, cardiac phased-array transducers) enable transducer manipulation in small anatomic areas (*e.g.*, intercostal spaces). For LUS, either curvilinear, microconvex or phased-array transducers may be used.

The choice of adequate ultrasound frequency is more important than the footprint. Piezoelectric material generates ultrasound waves in the MHz range, and the frequency affects ultrasound penetration and axial discrimination (*i.e.*, resolution). High frequency transducers allow higher axial resolution, and therefore better quality images; but are limited by low tissue penetration of ultrasound waves (and the opposite holds for low frequency transducers). Therefore, in choosing an ultrasound transducer for LUS examination, depth of structures and level of detail required are the most important considerations.[215] For example, the pleural line is best visualized with a high frequency (10 MHz) linear probe, whereas assessment of interstitial syndrome is better with lower frequency (1-5 MHz) (Table 1).

Measurements and Uses:

LUS can have substantial diagnostic impact in acute respiratory failure, with substantial capacity to reclassify lesions and change management;[216] the sensitivity and specificity for various conditions is illustrated (Table 2).[214,217-227]

Detection of real-time changes of LUS patterns and their correlation with different lung aeration conditions allows for bedside monitoring of injured lungs, and daily LUS can

reduce utilization of CXR and CT in the critically ill.[228] LUS predicted the distribution of lung aeration measured by CT in ARDS. [229] It can monitor lung re-aeration following management changes such treatment of pneumonia,[64] mechanical ventilation,[230] prone positioning,[231-233] recruitment maneuvers or changes in PEEP,180[180,234-236] re-aeration during extracorporeal membrane oxygenation,[237] and can identify tidal recruitment.[238] Indeed, aeration changes during the first hour of prone positioning may be a good predictor of successful response,[239] and formal assessment of lung recruitment yields similar results as with pressure-volume curves.[240] In addition, LUS can detect loss of aeration despite passing a spontaneous breathing trial, conferring a substantial risk of respiratory failure following extubation.[241,242]

B-lines are a sensitive marker of injury, appearing early with loss of lung aeration; in fact they appear before gas exchange deterioration in oleic-acid injury, and correlate with worsening of lung compliance.[243] They are an early and sensitive finding in lung contusion, [225] infection[244,245] and inflammation or fibrosis.[246] LUS examination of patients undergoing whole lung lavage for alveolar proteinosis demonstrated real-time increasing numbers of B-lines followed by development of consolidation; following lavage, the alveolar and interstitial syndromes resolved, reflecting re-aeration.[247] An analogous report documented real-time resolution of B-lines during hemodialysis.[169] The number of B-lines correlates with the amount of lost aeration[248] and with extra-vascular lung water, where the interstitial syndrome is caused by fluid accumulation.[249-250]

Several methods have been used to quantify the severity of alveolar-interstitial syndrome with LUS.[253-256] In critically ill patients, a semi-quantitative score reflecting loss of aeration (normally aerated lung: 0 point; moderate loss - B1: 1 point; severe loss - B2: 2 points; lung consolidation: 3 points) is commonly used.[230,241,242]

Detection of diffuse bilateral interstitial syndrome suggests the diagnosis of heart failure and performs well compared with CXR and natriuretic peptides.[256-260] In addition, severe loss of lung aeration (*i.e.*, alveolar syndrome) indicates consolidation (*e.g.*, pneumonia) or atelectasis (Table 2). Finally, the presence (and quantity) of interstitial syndrome may be prognostic in heart failure and in end-stage renal disease.[261,262]

Integrated approaches that utilize LUS (in the setting of multiorgan assessment) can increase the diagnostic yield for diagnosis of pulmonary embolism,[267] which may be useful when CT is contraindicated, and may clarify diagnosis in acute hypoxemic respiratory failure.[263] Addition of LUS findings to a modified version of the ARDS criteria suggested that it is feasible in resource-limited settings,[264] although this is context-sensitive.[265]

Finally, LUS most accurately detects pleural conditions such as pneumothorax and pleural effusion (Table 2). [214,227]

Challenges and Limitations:

While LUS is highly sensitive for several conditions (Table 2), in general the specificity is low, and this may be overcome by appreciation of advanced characteristics,[266] and by integration with the clinical context[259] and other imaging (*e.g.* radiography,

echocardiography).[267] Operator dependency is a concern, especially as the technique becomes more commonly used; while this may increase standards, it may also lead to inconsistent use. Adequate training[268,269] and use of standardized imaging protocols[25,270] will limit diagnostic error. It seems that 25 supervised LUS examinations may represent an adequate number to achieve minimal competence.[268] Although readily repeatable, LUS cannot be used continuously, nor can it be automated; this limits its use as a monitoring tool. Finally, although LUS accurately detects and quantifies lung recruitment, it cannot identify overdistension.

Emerging Developments:

Increased portability and lower cost have facilitated the use of LUS in non-traditional scenarios, such as in pre-hospital and resource-limited settings. LUS is already in use in under-resourced settings,[264] where conventional diagnostics are less available; this may promote a standardized approach to assessment of lung injury around the world. Development of tele-ultrasound will augment expansion of LUS,[271] and newer approaches to quantitation and automation[272] will likely increase use and acceptability. In ARDS, LUS could help categorize lung morphology at bedside and to assign treatment based on imaging phenotypes.[122]

Challenges and Limitations:

The major challenges to LUS may be the requirement for clinicians to learn the necessary additional skills, and this may be especially the case among clinicians who graduated and trained in the 'pre ultrasound' era. In addition, the capital equipment and transducers are still relatively expensive (total acquisition costs for versatile equipment may be approximately: $ 30-50,000), meaning that its availability may be limited. However, more affordable hand-held devices ($ 8-10,000) are now available and may further facilitate widespread use of this technology. In addition, some scenarios (*e.g.* obesity, surgical dressing) are not amenable to accurate imaging, and unavailable windows (*e.g.* behind the sternum or scapulae) represent significant limitations. Ultrasound-generated tissue damage is possible due to thermal and mechanical energy transfer;[273] lung hemorrhage has been reported in animal models. However, these effects are likely of limited clinical relevance within mandated limits of exposure and energy.[273]

Future Developments:

LUS may evolve into a powerful therapeutic tool. Commercially available microbubbles, that are routinely used as intravascular and tissue contrast for echocardiographic studies, undergo cavitation when exposed to higher energy ultrasound. This causes transient formation of pores and enhanced endocytosis through biological membranes, and can induce local uptake of drugs or genes.[274,275] In a murine experimental model of gram-negative pneumonia, LUS with microbubbles enhanced gentamicin delivery to injured lungs and increased bacterial killing.[276] This application of LUS could provide new therapeutic options for treatment of injured lungs. Finally, increase automation and sophistication of signal analysis may enable LUS to be eventually for continuous monitoring.

SUMMARY

Further research will reveal how conventional and advanced imaging techniques can be integrated in the care of patients with ARDS. Plain radiography, though nonspecific for lung injury, identifies patients with hypoxemic respiratory failure who are at risk to be further damaged by mechanical ventilation, and is useful as a screening tool. Diagnostic CT may be confirmatory, clarifies the distribution of injury, and may rule out alternative diagnoses. LUS is increasingly used at the bedside diagnosis; it is invaluable for guiding interventional procedures. Also, both EIT and LUS are promising in the determination of ventilation patterns and responses to respiratory maneuvers.

PET and MRI have improved our understanding of pulmonary function and biology; while they cannot yet be considered routine in the management of patients with ARDS, ongoing technological improvements will increase their accessibility and appeal.

Quantitative CT also shows great promise. As image processing techniques become more rapid and sophisticated, it is conceivable that CT characterization of potential for lung recruitment, strain, and micro heterogeneity of inflation could yield viable targets for individualized treatment. This is an important addition since clinical criteria do not anticipate the clinical trajectory and treatment response of an individual patient. With careful transport, dose-reducing protocols, and portable scanners future studies will establish whether or not the risk and cost of quantitative CT will be compensated by the ability to obtain substantial information and improve management.

Supplementary Material

Refer to Web version on PubMed Central for supplementary material.

Acknowledgments

REFERENCES

1. Ashbaugh DG, Bigelow DB, Petty TL, Levine BE: Acute respiratory distress in adults. Lancet 1967; 2: 319–323 [PubMed: 4143721]

2. Gattinoni L, Pesenti A: ARDS: the non-homogeneous lung; facts and hypotheses. Intensive and Crit Care Digest 1987; 6: 1–4

3. Elicker BM, Jones KT, Naeger DM, Frank JA: Imaging of Acute Lung Injury. Radiol Clin North Am 2016; 54: 1119–1132 [PubMed: 27719979]

4. Gattinoni L, Pesenti A, Avalli L, Rossi F, Bombino M: Pressure-volume curve of total respiratory system in acute respiratory failure. Computed tomographic scan study. Am Rev Respir Dis 1987; 136: 730–736 [PubMed: 3307572]

5. Puybasset L, Cluzel P, Chao N, Slutsky AS, Coriat P, Rouby JJ: A computed tomography scan assessment of regional lung volume in acute lung injury. The CT Scan ARDS Study Group. Am J Respir Crit Care Med 1998; 158: 1644–1655 [PubMed: 9817720]

6. Ventilation with lower tidal volumes as compared with traditional tidal volumes for acute lung injury and the acute respiratory distress syndrome. The Acute Respiratory Distress Syndrome Network. N Engl J Med 2000; 342: 1301–1308 [PubMed: 10793162]

7. Amato MB, Barbas CS, Medeiros DM, Magaldi RB, Schettino GP, Lorenzi-Filho G, Kairalla RA, Deheinzelin D, Munoz C, Oliveira R, Takagaki TY, Carvalho CR: Effect of a protective-ventilation strategy on mortality in the acute respiratory distress syndrome. N Engl J Med 1998; 338: 347–354 [PubMed: 9449727]

8. Bryan AC: Conference on the scientific basis of respiratory therapy. Pulmonary physiotherapy in the pediatric age group. Comments of a devil's advocate. Am Rev Respir Dis 1974; 110: 143–144 [PubMed: 4440945]

9. Gattinoni L, Pelosi P, Vitale G, Pesenti A, D'Andrea L, Mascheroni D: Body position changes redistribute lung computed-tomographic density in patients with acute respiratory failure. Anesthesiology 1991; 74: 15–23 [PubMed: 1986640]

10. Gattinoni L, Pelosi P, Crotti S, Valenza F: Effects of positive end-expiratory pressure on regional distribution of tidal volume and recruitment in adult respiratory distress syndrome. Am J Respir Crit Care Med 1995; 151: 1807–1814 [PubMed: 7767524]

11. Dambrosio M, Roupie E, Mollet JJ, Anglade MC, Vasile N, Lemaire F, Brochard L: Effects of positive end-expiratory pressure and different tidal volumes on alveolar recruitment and hyperinflation. Anesthesiology 1997; 87: 495–503 [PubMed: 9316952]

12. Bellani G, Guerra L, Musch G, Zanella A, Patroniti N, Mauri T, Messa C, Pesenti A: Lung regional metabolic activity and gas volume changes induced by tidal ventilation in patients with acute lung injury. Am J Respir Crit Care Med 2011; 183: 1193–1199 [PubMed: 21257791]

13. Borges JB, Costa EL, Bergquist M, Lucchetta L, Widstrom C, Maripuu E, Suarez-Sipmann F, Larsson A, Amato MB, Hedenstierna G: Lung inflammation persists after 27 hours of protective Acute Respiratory Distress Syndrome Network Strategy and is concentrated in the nondependent lung. Crit Care Med 2015; 43: e123–32 [PubMed: 25746507]

14. Cereda M, Xin Y, Hamedani H, Bellani G, Kadlecek S, Clapp J, Guerra L, Meeder N, Rajaei J, Tustison NJ, Gee JC, Kavanagh BP, Rizi RR: Tidal changes on CT and progression of ARDS. Thorax 2017; 72: 981–989 [PubMed: 28634220]

15. Cressoni M, Cadringher P, Chiurazzi C, Amini M, Gallazzi E, Marino A, Brioni M, Carlesso E, Chiumello D, Quintel M, Bugedo G, Gattinoni L: Lung inhomogeneity in patients with acute respiratory distress syndrome. Am J Respir Crit Care Med 2014; 189: 149–158 [PubMed: 24261322]

16. Cereda M, Emami K, Xin Y, Kadlecek S, Kuzma NN, Mongkolwisetwara P, Profka H, Pickup S, Ishii M, Kavanagh BP, Deutschman CS, Rizi RR: Imaging the interaction of atelectasis and overdistension in surfactant-depleted lungs. Crit Care Med 2013; 41: 527–535 [PubMed: 23263577]

17. Mead J, Takishima T, Leith D: Stress distribution in lungs: a model of pulmonary elasticity. J Appl Physiol 1970; 28: 596–608 [PubMed: 5442255]

18. Schiller HJ, McCann UG 2nd, Carney DE, Gatto LA, Steinberg JM, Nieman GF: Altered alveolar mechanics in the acutely injured lung. Crit Care Med 2001; 29: 1049–1055 [PubMed: 11383531]

19. Papazian L, Calfee CS, Chiumello D, Luyt CE, Meyer NJ, Sekiguchi H, Matthay MA, Meduri GU: Diagnostic workup for ARDS patients. Intensive Care Med 2016; 42: 674–685 [PubMed: 27007111]

20. Goffi A, Kruisselbrink R, Volpicelli G: The sound of air: point-of-care lung ultrasound in perioperative medicine. Can J Anaesth 2018; 65: 399–416 [PubMed: 29411300]

21. Adler A, Boyle A: Electrical Impedance Tomography: Tissue Properties to Image Measures. IEEE Trans Biomed Eng 2017; 64: 2494–2504 [PubMed: 28715324]

22. Frerichs I, Amato MB, van Kaam AH, Tingay DG, Zhao Z, Grychtol B, Bodenstein M, Gagnon H, Bohm SH, Teschner E, Stenqvist O, Mauri T, Torsani V, Camporota L, Schibler A, Wolf GK, Gommers D, Leonhardt S, Adler A: Chest electrical impedance tomography examination, data analysis, terminology, clinical use and recommendations: consensus statement of the Translational EIT development study group. Thorax 2017; 72: 83–93 [PubMed: 27596161]

23. Costa EL, Lima RG, Amato MB: Electrical impedance tomography. Curr Opin Crit Care 2009; 15: 18–24 [PubMed: 19186406]

24. Costa EL, Borges JB, Melo A, Suarez-Sipmann F, Toufen C Jr., Bohm SH, Amato MB: Bedside estimation of recruitable alveolar collapse and hyperdistension by electrical impedance tomography. Intensive Care Med 2009; 35: 1132–7 [PubMed: 19255741]

25. Kruisselbrink R, Chan V, Cibinel GA, Abrahamson S, Goffi A: I-AIM (Indication, Acquisition, Interpretation, Medical Decision-making) Framework for Point of Care Lung Ultrasound. Anesthesiology 2017; 127: 568–582 [PubMed: 28742530]

26. Volpicelli G, Elbarbary M, Blaivas M, Lichtenstein DA, Mathis G, Kirkpatrick AW, Melniker L, Gargani L, Noble VE, Via G, Dean A, Tsung JW, Soldati G, Copetti R, Bouhemad B, Reissig A, Agricola E, Rouby JJ, Arbelot C, Liteplo A, Sargsyan A, Silva F, Hoppmann R, Breitkreutz R, Seibel A, Neri L, Storti E, Petrovic T, International Liaison Committee on Lung Ultrasound for International Consensus Conference on Lung U: International evidence-based recommendations for point-of-care lung ultrasound. Intensive Care Med 2012; 38: 577–91 [PubMed: 22392031]

27. Cereda M, Emami K, Kadlecek S, Xin Y, Mongkolwisetwara P, Profka H, Barulic A, Pickup S, Mansson S, Wollmer P, Ishii M, Deutschman CS, Rizi RR: Quantitative imaging of alveolar recruitment with hyperpolarized gas MRI during mechanical ventilation. J Appl Physiol 2011; 110: 499–511 [PubMed: 21127207]

28. Mugler JP 3rd, Altes TA, Ruset IC, Dregely IM, Mata JF, Miller GW, Ketel S, Ketel J, Hersman FW, Ruppert K: Simultaneous magnetic resonance imaging of ventilation distribution and gas uptake in the human lung using hyperpolarized xenon-129. Proc Natl Acad Sci U S A 2010; 107: 21707–12 [PubMed: 21098267]

29. Ruppert K, Hamedani H, Amzajerdian F, Xin Y, Duncan IF, Profka H, Siddiqui S, Pourfathi M, Kadlecek S, Rizi RR: Assessment of Pulmonary Gas Transport in Rabbits Using Hyperpolarized Xenon-129 Magnetic Resonance Imaging. Sci Rep 2018; 8: 7310 [PubMed: 29743565]

30. Pourfathi M, Cereda M, Chatterjee S, Xin Y, Kadlecek S, Duncan I, Hamedani H, Siddiqui S, Profka H, Ehrich J, Ruppert K, Rizi RR: Lung Metabolism and Inflammation during Mechanical Ventilation; An Imaging Approach. Sci Rep 2018; 8: 3525 [PubMed: 29476083]

31. Thind K, Jensen MD, Hegarty E, Chen AP, Lim H, Martinez-Santiesteban F, Van Dyk J, Wong E, Scholl TJ, Santyr GE: Mapping metabolic changes associated with early Radiation Induced Lung Injury post conformal radiotherapy using hyperpolarized (13)C-pyruvate Magnetic Resonance Spectroscopic Imaging. Radiother Oncol 2014; 110: 317–322 [PubMed: 24440041]

32. Ferguson ND, Fan E, Camporota L, Antonelli M, Anzueto A, Beale R, Brochard L, Brower R, Esteban A, Gattinoni L, Rhodes A, Slutsky AS, Vincent JL, Rubenfeld GD, Thompson BT, Ranieri VM: The Berlin definition of ARDS: an expanded rationale, justification, and supplementary material. Intensive Care Med 2012; 38: 1573–82 [PubMed: 22926653]

33. Calfee CS, Delucchi K, Parsons PE, Thompson BT, Ware LB, Matthay MA, Network NA: Subphenotypes in acute respiratory distress syndrome: latent class analysis of data from two randomised controlled trials. Lancet Respir Med 2014; 2: 611–20 [PubMed: 24853585]

34. Goligher EC, Kavanagh BP, Rubenfeld GD, Adhikari NK, Pinto R, Fan E, Brochard LJ, Granton JT, Mercat A, Marie Richard JC, Chretien JM, Jones GL, Cook DJ, Stewart TE, Slutsky AS, Meade MO, Ferguson ND: Oxygenation response to positive end-expiratory pressure predicts mortality in acute respiratory distress syndrome. A secondary analysis of the LOVS and ExPress trials. Am J Respir Crit Care Med 2014; 190: 70–6 [PubMed: 24919111]

35. Famous KR, Delucchi K, Ware LB, Kangelaris KN, Liu KD, Thompson BT, Calfee CS, Network A: Acute Respiratory Distress Syndrome Subphenotypes Respond Differently to Randomized Fluid Management Strategy. Am J Respir Crit Care Med 2017; 195: 331–338 [PubMed: 27513822]

36. Rubenfeld GD: Confronting the frustrations of negative clinical trials in acute respiratory distress syndrome. Ann Am Thorac Soc 2015; 12 Suppl 1: S58–63 [PubMed: 25830838]

37. Laffey JG, Kavanagh BP: Fifty Years of Research in ARDS. Insight into Acute Respiratory Distress Syndrome. From Models to Patients. Am J Respir Crit Care Med 2017; 196: 18–28 [PubMed: 28146637]

38. Bernard GR, Artigas A, Brigham KL, Carlet J, Falke K, Hudson L, Lamy M, Legall JR, Morris A, Spragg R: The American-European Consensus Conference on ARDS. Definitions, mechanisms,

relevant outcomes, and clinical trial coordination. Am J Respir Crit Care Med 1994; 149: 818–824 [PubMed: 7509706]

39. Force ADT, Ranieri VM, Rubenfeld GD, Thompson BT, Ferguson ND, Caldwell E, Fan E, Camporota L, Slutsky AS: Acute respiratory distress syndrome: the Berlin Definition. JAMA : the journal of the American Medical Association 2012; 307: 2526–2533 [PubMed: 22797452]

40. Murray JF, Matthay MA, Luce JM, Flick MR: An expanded definition of the adult respiratory distress syndrome. Am Rev Respir Dis 1988; 138: 720–723 [PubMed: 3202424]

41. Goodman PC: Radiographic findings in patients with acute respiratory distress syndrome. Clin Chest Med 2000; 21: 419–33, vii [PubMed: 11019718]

42. Lichtenstein D, Goldstein I, Mourgeon E, Cluzel P, Grenier P, Rouby JJ: Comparative diagnostic performances of auscultation, chest radiography, and lung ultrasonography in acute respiratory distress syndrome. Anesthesiology 2004; 100: 9–15 [PubMed: 14695718]

43. Figueroa-Casas JB, Brunner N, Dwivedi AK, Ayyappan AP: Accuracy of the chest radiograph to identify bilateral pulmonary infiltrates consistent with the diagnosis of acute respiratory distress syndrome using computed tomography as reference standard. J Crit Care 2013; 28: 352–7 [PubMed: 23566733]

44. Schmickl CN, Pannu S, Al-Qadi MO, Alsara A, Kashyap R, Dhokarh R, Herasevich V, Gajic O: Decision support tool for differential diagnosis of Acute Respiratory Distress Syndrome (ARDS) vs Cardiogenic Pulmonary Edema (CPE): a prospective validation and meta-analysis. Crit Care 2014; 18: 659 [PubMed: 25432274]

45. Ferguson ND, Frutos-Vivar F, Esteban A, Fernandez-Segoviano P, Aramburu JA, Najera L, Stewart TE: Acute respiratory distress syndrome: underrecognition by clinicians and diagnostic accuracy of three clinical definitions. Crit Care Med 2005; 33: 2228–2234 [PubMed: 16215375]

46. Lorente JA, Cardinal-Fernandez P, Munoz D, Frutos-Vivar F, Thille AW, Jaramillo C, Ballen-Barragan A, Rodriguez JM, Penuelas O, Ortiz G, Blanco J, Pinheiro BV, Nin N, del Carmen Marin M, Esteban A, Thompson TB: Acute respiratory distress syndrome in patients with and without diffuse alveolar damage: an autopsy study. Intensive Care Med 2015; 41: 1921–30 [PubMed: 26385863]

47. Thille AW, Esteban A, Fernandez-Segoviano P, Rodriguez JM, Aramburu JA, Penuelas O, Cortes-Puch I, Cardinal-Fernandez P, Lorente JA, Frutos-Vivar F: Comparison of the Berlin definition for acute respiratory distress syndrome with autopsy. Am J Respir Crit Care Med 2013; 187: 761–7 [PubMed: 23370917]

48. Rubenfeld GD, Caldwell E, Granton J, Hudson LD, Matthay MA: Interobserver variability in applying a radiographic definition for ARDS. Chest 1999; 116: 1347–1353 [PubMed: 10559098]

49. Meade MO, Cook RJ, Guyatt GH, Groll R, Kachura JR, Bedard M, Cook DJ, Slutsky AS, Stewart TE: Interobserver variation in interpreting chest radiographs for the diagnosis of acute respiratory distress syndrome. Am J Respir Crit Care Med 2000; 161: 85–90 [PubMed: 10619802]

50. Sjoding MW, Hofer TP, Co I, Courey A, Cooke CR, Iwashyna TJ: Interobserver Reliability of the Berlin ARDS Definition and Strategies to Improve the Reliability of ARDS Diagnosis. Chest 2018; 153: 361–367 [PubMed: 29248620]

51. Goddard SL, Rubenfeld GD, Manoharan V, Dev SP, Laffey J, Bellani G, Pham T, Fan E: The Randomized Educational Acute Respiratory Distress Syndrome Diagnosis Study: A Trial to Improve the Radiographic Diagnosis of Acute Respiratory Distress Syndrome. Crit Care Med 2018; 46: 743–748 [PubMed: 29438110]

52. Herasevich V, Yilmaz M, Khan H, Hubmayr RD, Gajic O: Validation of an electronic surveillance system for acute lung injury. Intensive Care Med 2009; 35: 1018–23 [PubMed: 19280175]

53. Rajpurkar P, Irvin J, Zhu K, Yang B, Mehta H, Duan T, Ding D, Bagul A, Langlotz C, Shpanskaya K, Lungren MP, Ng AY: CheXNet: Radiologist-Level Pneumonia Detection on Chest X-Rays with Deep Learning. arXiv:1711.05225 [cs, stat] 2017

54. Wang X, Peng Y, Lu L, Lu Z, Bagheri M, Summers RM: ChestX-ray8: Hospital-scale Chest X-ray Database and Benchmarks on Weakly-Supervised Classification and Localization of Common Thorax Diseases. arXiv:1705.02315 [cs] 2017

55. Simon BA, Kaczka DW, Bankier AA, Parraga G: What can computed tomography and magnetic resonance imaging tell us about ventilation? J Appl Physiol (1985) 2012; 113: 647–57 [PubMed: 22653989]

56. Kaczka DW, Cao K, Christensen GE, Bates JH, Simon BA: Analysis of regional mechanics in canine lung injury using forced oscillations and 3D image registration. Annals of Biomedical Engineering 2011; 39: 1112–1124 [PubMed: 21132371]

57. Reinhardt JM, Christensen GE, Hoffman EA, Ding K, Cao K: Registration-derived estimates of local lung expansion as surrogates for regional ventilation. Inf Process Med Imaging 2007; 20: 763–74 [PubMed: 17633746]

58. Reinhardt JM, Ding K, Cao K, Christensen GE, Hoffman EA, Bodas SV: Registration-based estimates of local lung tissue expansion compared to xenon CT measures of specific ventilation. Med Image Anal 2008; 12: 752–63 [PubMed: 18501665]

59. Simon M, Braune S, Laqmani A, Metschke M, Berliner C, Kalsow M, Klose H, Kluge S: Value of Computed Tomography of the Chest in Subjects With ARDS: A Retrospective Observational Study. Respir Care 2016; 61: 316–23 [PubMed: 26647453]

60. Miller WT Jr., Tino G, Friedburg JS: Thoracic CT in the intensive care unit: assessment of clinical usefulness. Radiology 1998; 209: 491–8 [PubMed: 9807579]

61. Hansell DM, Bankier AA, MacMahon H, McLoud TC, Muller NL, Remy J: Fleischner Society: glossary of terms for thoracic imaging. Radiology 2008; 246: 697–722 [PubMed: 18195376]

62. Winer-Muram HT, Steiner RM, Gurney JW, Shah R, Jennings SG, Arheart KL, Eltorky MA, Meduri GU: Ventilator-associated pneumonia in patients with adult respiratory distress syndrome: CT evaluation. Radiology 1998; 208: 193–9 [PubMed: 9646813]

63. Miller WT Jr., Panosian JS: Causes and imaging patterns of tree-in-bud opacities. Chest 2013; 144: 1883–1892 [PubMed: 23948769]

64. Bouhemad B, Liu ZH, Arbelot C, Zhang M, Ferarri F, Le-Guen M, Girard M, Lu Q, Rouby JJ: Ultrasound assessment of antibiotic-induced pulmonary reaeration in ventilator-associated pneumonia. Crit Care Med 2010; 38: 84–92 [PubMed: 19633538]

65. Gibelin A, Parrot A, Maitre B, Brun-Buisson C, Mekontso Dessap A, Fartoukh M, de Prost N: Acute respiratory distress syndrome mimickers lacking common risk factors of the Berlin definition. Intensive Care Med 2016; 42: 164–72 [PubMed: 26408150]

66. Tagliabue M, Casella TC, Zincone GE, Fumagalli R, Salvini E: CT and chest radiography in the evaluation of adult respiratory distress syndrome. Acta Radiol 1994; 35: 230–4 [PubMed: 8192958]

67. Gattinoni L, Bombino M, Pelosi P, Lissoni A, Pesenti A, Fumagalli R, Tagliabue M: Lung structure and function in different stages of severe adult respiratory distress syndrome. JAMA : the journal of the American Medical Association 1994; 271: 1772–1779 [PubMed: 8196122]

68. Nieszkowska A, Lu Q, Vieira S, Elman M, Fetita C, Rouby JJ: Incidence and regional distribution of lung overinflation during mechanical ventilation with positive end-expiratory pressure. Crit Care Med 2004; 32: 1496–1503 [PubMed: 15241094]

69. Chung JH, Kradin RL, Greene RE, Shepard JA, Digumarthy SR: CT predictors of mortality in pathology confirmed ARDS. Eur Radiol 2011; 21: 730–7 [PubMed: 20927526]

70. Ichikado K, Muranaka H, Gushima Y, Kotani T, Nader HM, Fujimoto K, Johkoh T, Iwamoto N, Kawamura K, Nagano J, Fukuda K, Hirata N, Yoshinaga T, Ichiyasu H, Tsumura S, Kohrogi H, Kawaguchi A, Yoshioka M, Sakuma T, Suga M: Fibroproliferative changes on high-resolution CT in the acute respiratory distress syndrome predict mortality and ventilator dependency: a prospective observational cohort study. BMJ Open 2012; 2: e000545

71. Xin Y, Song G, Cereda M, Kadlecek S, Hamedani H, Jiang Y, Rajaei J, Clapp J, Profka H, Meeder N, Wu J, Tustison NJ, Gee JC, Rizi RR: Semiautomatic segmentation of longitudinal computed tomography images in a rat model of lung injury by surfactant depletion. J Appl Physiol (1985) 2015; 118: 377–85 [PubMed: 25640150]

72. Gerard SE, Herrmann J, Kaczka DW, Reinhardt JM: Transfer Learning for Segmentation of Injured Lungs Using Coarse-to-Fine Convolutional Neural Networks. Cham, Springer International Publishing, 2018, pp 191–201

73. van Rikxoort EM, van Ginneken B: Automated segmentation of pulmonary structures in thoracic computed tomography scans: a review. Phys Med Biol 2013; 58: R187–220 [PubMed: 23956328]

74. Denison DM, Morgan MD, Millar AB: Estimation of regional gas and tissue volumes of the lung in supine man using computed tomography. Thorax 1986; 41: 620–628 [PubMed: 3787544]

75. Wandtke JC, Hyde RW, Fahey PJ, Utell MJ, Plewes DB, Goske MJ, Fischer HW: Measurement of lung gas volume and regional density by computed tomography in dogs. Investigative radiology 1986; 21: 108–117 [PubMed: 3957586]

76. Cressoni M, Gallazzi E, Chiurazzi C, Marino A, Brioni M, Menga F, Cigada I, Amini M, Lemos A, Lazzerini M, Carlesso E, Cadringher P, Chiumello D, Gattinoni L: Limits of normality of quantitative thoracic CT analysis. Crit Care 2013; 17: R93 [PubMed: 23706034]

77. Vieira SR, Puybasset L, Richecoeur J, Lu Q, Cluzel P, Gusman PB, Coriat P, Rouby JJ: A lung computed tomographic assessment of positive end-expiratory pressure-induced lung overdistension. Am J Respir Crit Care Med 1998; 158: 1571–1577 [PubMed: 9817710]

78. Malbouisson LM, Muller JC, Constantin JM, Lu Q, Puybasset L, Rouby JJ, Group CTSAS: Computed tomography assessment of positive end-expiratory pressure-induced alveolar recruitment in patients with acute respiratory distress syndrome. Am J Respir Crit Care Med 2001; 163: 1444–1450 [PubMed: 11371416]

79. Ochs M, Nyengaard JR, Jung A, Knudsen L, Voigt M, Wahlers T, Richter J, Gundersen HJ: The number of alveoli in the human lung. Am J Respir Crit Care Med 2004; 169: 120–4 [PubMed: 14512270]

80. Yin Y, Hoffman EA, Ding K, Reinhardt JM, Lin CL: A cubic B-spline-based hybrid registration of lung CT images for a dynamic airway geometric model with large deformation. Phys Med Biol 2011; 56: 203–18 [PubMed: 21149947]

81. Christensen GE, Song JH, Lu W, El Naqa I, Low DA: Tracking lung tissue motion and expansion/compression with inverse consistent image registration and spirometry. Med Phys 2007; 34: 2155–63 [PubMed: 17654918]

82. Avants BB, Tustison NJ, Song G, Cook PA, Klein A, Gee JC: A reproducible evaluation of ANTs similarity metric performance in brain image registration. NeuroImage 2011; 54: 2033–2044 [PubMed: 20851191]

83. Yin Y, Hoffman EA, Lin CL: Mass preserving nonrigid registration of CT lung images using cubic B-spline. Med Phys 2009; 36: 4213–22 [PubMed: 19810495]

84. Li B, Christensen GE, Hoffman EA, McLennan G, Reinhardt JM: Pulmonary CT image registration and warping for tracking tissue deformation during the respiratory cycle through 3D consistent image registration. Med Phys 2008; 35: 5575–83 [PubMed: 19175115]

85. Herrmann J, Hoffman EA, Kaczka DW: Frequency-Selective Computed Tomography: Applications During Periodic Thoracic Motion. IEEE Trans Med Imaging 2017; 36: 1722–1732 [PubMed: 28436852]

86. Bruhn A, Bugedo D, Riquelme F, Varas J, Retamal J, Besa C, Cabrera C, Bugedo G: Tidal volume is a major determinant of cyclic recruitment-derecruitment in acute respiratory distress syndrome. Minerva Anestesiol 2011; 77: 418–26 [PubMed: 21483386]

87. Zhao B, Christensen GE, Song JH, Pan Y, Gerard SE, Reinhardt JM, Du K, Patton T, Bayouth JM, Hugo JD: Tissue-volume preserving deformable image registration for 4DCT pulmonary images. 2016 IEEE Conference on Computer Vision and Pattern Recognition Workshops 2016: 41–49

88. Murphy K, van Ginneken B, Reinhardt JM, Kabus S, Ding K, Deng X, Cao K, Du K, Christensen GE, Garcia V, Vercauteren T, Ayache N, Commowick O, Malandain G, Glocker B, Paragios N, Navab N, Gorbunova V, Sporring J, de Bruijne M, Han X, Heinrich MP, Schnabel JA, Jenkinson M, Lorenz C, Modat M, McClelland JR, Ourselin S, Muenzing SE, Viergever MA, De Nigris D, Collins DL, Arbel T, Peroni M, Li R, Sharp GC, Schmidt-Richberg A, Ehrhardt J, Werner R, Smeets D, Loeckx D, Song G, Tustison N, Avants B, Gee JC, Staring M, Klein S, Stoel BC, Urschler M, Werlberger M, Vandemeulebroucke J, Rit S, Sarrut D, Pluim JP: Evaluation of registration methods on thoracic CT: the EMPIRE10 challenge. IEEE Trans Med Imaging 2011; 30: 1901–1920 [PubMed: 21632295]

89. Hu S, Hoffman EA, Reinhardt JM: Automatic lung segmentation for accurate quantitation of volumetric X-ray CT images. IEEE Trans Med Imaging 2001; 20: 490–8 [PubMed: 11437109]

90. Chon D, Beck KC, Simon BA, Shikata H, Saba OI, Hoffman EA: Effect of low-xenon and krypton supplementation on signal/noise of regional CT-based ventilation measurements. J Appl Physiol 2007; 102: 1535–1544 [PubMed: 17122371]

91. Chon D, Simon BA, Beck KC, Shikata H, Saba OI, Won C, Hoffman EA: Differences in regional wash-in and wash-out time constants for xenon-CT ventilation studies. Respir Physiol Neurobiol 2005; 148: 65–83 [PubMed: 16061426]

92. Hoegl S, Meinel FG, Thieme SF, Johnson TR, Eickelberg O, Zwissler B, Nikolaou K: Worsening respiratory function in mechanically ventilated intensive care patients: feasibility and value of xenon-enhanced dual energy CT. Eur J Radiol 2013; 82: 557–62 [PubMed: 23238360]

93. Fuld MK, Halaweish AF, Newell JD, Krauss B, Hoffman EA: Optimization of dual-energy xenon-computed tomography for quantitative assessment of regional pulmonary ventilation. Invest Radiol 2013; 48: 629–637 [PubMed: 23571834]

94. Lee YY, Muchhal K, Chan CK, Cheung AS: Levobupivacaine and fentanyl for spinal anaesthesia: a randomized trial. Eur J Anaesthesiol 2005; 22: 899–903 [PubMed: 16318658]

95. Kong X, Sheng HX, Lu GM, Meinel FG, Dyer KT, Schoepf UJ, Zhang LJ: Xenon-enhanced dual-energy CT lung ventilation imaging: techniques and clinical applications. AJR Am J Roentgenol 2014; 202: 309–17 [PubMed: 24450670]

96. Bayat S, Le Duc G, Porra L, Berruyer G, Nemoz C, Monfraix S, Fiedler S, Thomlinson W, Suortti P, Standertskjold-Nordenstam CG, Sovijarvi AR: Quantitative functional lung imaging with synchrotron radiation using inhaled xenon as contrast agent. Phys Med Biol 2001; 46: 3287–99 [PubMed: 11768506]

97. Bayat S, Porra L, Suhonen H, Janosi T, Strengell S, Habre W, Petak F, Hantos Z, Suortti P, Sovijarvi A: Imaging of lung function using synchrotron radiation computed tomography: what's new? Eur J Radiol 2008; 68: S78–83 [PubMed: 18606518]

98. Deman P, Tan S, Belev G, Samadi N, Martinson M, Chapman D, Ford NL: Respiratory-gated KES imaging of a rat model of acute lung injury at the Canadian Light Source. Journal of Synchrotron Radiation; 24: 679–685 [PubMed: 28452761]

99. Gattinoni L, D'Andrea L, Pelosi P, Vitale G, Pesenti A, Fumagalli R: Regional effects and mechanism of positive end-expiratory pressure in early adult respiratory distress syndrome. JAMA 1993; 269: 2122–7 [PubMed: 8468768]

100. Pelosi P, D'Andrea L, Vitale G, Pesenti A, Gattinoni L: Vertical gradient of regional lung inflation in adult respiratory distress syndrome. Am J Respir Crit Care Med 1994; 149: 8–13 [PubMed: 8111603]

101. Pelosi P, Goldner M, McKibben A, Adams A, Eccher G, Caironi P, Losappio S, Gattinoni L, Marini JJ: Recruitment and derecruitment during acute respiratory failure: an experimental study. Am J Respir Crit Care Med 2001; 164: 122–130 [PubMed: 11435250]

102. Malbouisson LM, Busch CJ, Puybasset L, Lu Q, Cluzel P, Rouby JJ: Role of the heart in the loss of aeration characterizing lower lobes in acute respiratory distress syndrome. CT Scan ARDS Study Group. Am J Respir Crit Care Med 2000; 161: 2005–2012 [PubMed: 10852781]

103. Hubmayr RD, Walters BJ, Chevalier PA, Rodarte JR, Olson LE: Topographical distribution of regional lung volume in anesthetized dogs. J Appl Physiol 1983; 54: 1048–1056 [PubMed: 6853280]

104. Pelosi P, Cereda M, Foti G, Giacomini M, Pesenti A: Alterations of lung and chest wall mechanics in patients with acute lung injury: effects of positive end-expiratory pressure. Am J Respir Crit Care Med 1995; 152: 531–537 [PubMed: 7633703]

105. Terragni PP, Rosboch G, Tealdi A, Corno E, Menaldo E, Davini O, Gandini G, Herrmann P, Mascia L, Quintel M, Slutsky AS, Gattinoni L, Ranieri VM: Tidal hyperinflation during low tidal volume ventilation in acute respiratory distress syndrome. Am J Respir Crit Care Med 2007; 175: 160–166 [PubMed: 17038660]

106. Mattingley JS, Holets SR, Oeckler RA, Stroetz RW, Buck CF, Hubmayr RD: Sizing the lung of mechanically ventilated patients. Crit Care 2011; 15: R60 [PubMed: 21320330]

107. Amato MB, Meade MO, Slutsky AS, Brochard L, Costa EL, Schoenfeld DA, Stewart TE, Briel M, Talmor D, Mercat A, Richard JC, Carvalho CR, Brower RG: Driving pressure and survival in the acute respiratory distress syndrome. N Engl J Med 2015; 372: 747–55 [PubMed: 25693014]

108. Vieira SR, Puybasset L, Lu Q, Richecoeur J, Cluzel P, Coriat P, Rouby JJ: A scanographic assessment of pulmonary morphology in acute lung injury. Significance of the lower inflection point detected on the lung pressure-volume curve. Am J Respir Crit Care Med 1999; 159: 1612–1623 [PubMed: 10228135]

109. Gattinoni L, Caironi P, Cressoni M, Chiumello D, Ranieri VM, Quintel M, Russo S, Patroniti N, Cornejo R, Bugedo G: Lung recruitment in patients with the acute respiratory distress syndrome. N Engl J Med 2006; 354: 1775–1786 [PubMed: 16641394]

110. Crotti S, Mascheroni D, Caironi P, Pelosi P, Ronzoni G, Mondino M, Marini JJ, Gattinoni L: Recruitment and derecruitment during acute respiratory failure: a clinical study. Am J Respir Crit Care Med 2001; 164: 131–140 [PubMed: 11435251]

111. Otto CM, Markstaller K, Kajikawa O, Karmrodt J, Syring RS, Pfeiffer B, Good VP, Frevert CW, Baumgardner JE: Spatial and temporal heterogeneity of ventilator-associated lung injury after surfactant depletion. J Appl Physiol 2008; 104: 1485–1494 [PubMed: 18323462]

112. Tremblay LN, Slutsky AS: Ventilator-induced lung injury: from the bench to the bedside. Intensive Care Med 2006; 32: 24–33 [PubMed: 16231069]

113. Writing Group for the Alveolar Recruitment for Acute Respiratory Distress Syndrome Trial I, Cavalcanti AB, Suzumura EA, Laranjeira LN, Paisani DM, Damiani LP, Guimaraes HP, Romano ER, Regenga MM, Taniguchi LNT, Teixeira C, Pinheiro de Oliveira R, Machado FR, Diaz-Quijano FA, Filho MSA, Maia IS, Caser EB, Filho WO, Borges MC, Martins PA, Matsui M, Ospina-Tascon GA, Giancursi TS, Giraldo-Ramirez ND, Vieira SRR, Assef M, Hasan MS, Szczeklik W, Rios F, Amato MBP, Berwanger O, Ribeiro de Carvalho CR: Effect of Lung Recruitment and Titrated Positive End-Expiratory Pressure (PEEP) vs Low PEEP on Mortality in Patients With Acute Respiratory Distress Syndrome: A Randomized Clinical Trial. JAMA 2017; 318: 1335–1345 [PubMed: 28973363]

114. Constantin JM, Grasso S, Chanques G, Aufort S, Futier E, Sebbane M, Jung B, Gallix B, Bazin JE, Rouby JJ, Jaber S: Lung morphology predicts response to recruitment maneuver in patients with acute respiratory distress syndrome. Crit Care Med 2010; 38: 1108–17 [PubMed: 20154600]

115. Galiatsou E, Kostanti E, Svarna E, Kitsakos A, Koulouras V, Efremidis SC, Nakos G: Prone position augments recruitment and prevents alveolar overinflation in acute lung injury. Am J Respir Crit Care Med 2006; 174: 187–97 [PubMed: 16645177]

116. Cornejo RA, Diaz JC, Tobar EA, Bruhn AR, Ramos CA, Gonzalez RA, Repetto CA, Romero CM, Galvez LR, Llanos O, Arellano DH, Neira WR, Diaz GA, Zamorano AJ, Pereira GL: Effects of prone positioning on lung protection in patients with acute respiratory distress syndrome. Am J Respir Crit Care Med 2013; 188: 440–8 [PubMed: 23348974]

117. Guerin C, Reignier J, Richard JC, Beuret P, Gacouin A, Boulain T, Mercier E, Badet M, Mercat A, Baudin O, Clavel M, Chatellier D, Jaber S, Rosselli S, Mancebo J, Sirodot M, Hilbert G, Bengler C, Richecoeur J, Gainnier M, Bayle F, Bourdin G, Leray V, Girard R, Baboi L, Ayzac L, Group PS: Prone positioning in severe acute respiratory distress syndrome. N Engl J Med 2013; 368: 2159–2168 [PubMed: 23688302]

118. Mrozek S, Jabaudon M, Jaber S, Paugam-Burtz C, Lefrant JY, Rouby JJ, Asehnoune K, Allaouchiche B, Baldesi O, Leone M, Lu Q, Bazin JE, Roszyk L, Sapin V, Futier E, Pereira B, Constantin JM, Azurea n: Elevated Plasma Levels of sRAGE Are Associated With Nonfocal CT-Based Lung Imaging in Patients With ARDS: A Prospective Multicenter Study. Chest 2016; 150: 998–1007 [PubMed: 27018314]

119. Goodman LR, Fumagalli R, Tagliabue P, Tagliabue M, Ferrario M, Gattinoni L, Pesenti A: Adult respiratory distress syndrome due to pulmonary and extrapulmonary causes: CT, clinical, and functional correlations. Radiology 1999; 213: 545–552 [PubMed: 10551239]

120. Puybasset L, Gusman P, Muller JC, Cluzel P, Coriat P, Rouby JJ: Regional distribution of gas and tissue in acute respiratory distress syndrome. III. Consequences for the effects of positive end-expiratory pressure. CT Scan ARDS Study Group. Adult Respiratory Distress Syndrome. Intensive Care Med 2000; 26: 1215–1227 [PubMed: 11089745]

121. Rouby JJ, Puybasset L, Cluzel P, Richecoeur J, Lu Q, Grenier P: Regional distribution of gas and tissue in acute respiratory distress syndrome. II. Physiological correlations and definition of an ARDS Severity Score. CT Scan ARDS Study Group. Intensive Care Med 2000; 26: 1046–1056 [PubMed: 11030160]

122. Jabaudon M, Godet T, Futier E, Bazin JE, Sapin V, Roszyk L, Pereira B, Constantin JM, group A: Rationale, study design and analysis plan of the lung imaging morphology for ventilator settings in acute respiratory distress syndrome study (LIVE study): Study protocol for a randomised controlled trial. Anaesth Crit Care Pain Med 2017; 36: 301–306 [PubMed: 28323236]

123. Kano S, Lanteri CJ, Duncan AW, Sly PD: Influence of nonlinearities on estimates of respiratory mechanics using multilinear regression analysis. J Appl Physiol 1994; 77: 1185–1197 [PubMed: 7836121]

124. Carvalho AR, Pacheco SA, de Souza Rocha PV, Bergamini BC, Paula LF, Jandre FC, Giannella-Neto A: Detection of tidal recruitment/overdistension in lung-healthy mechanically ventilated patients under general anesthesia. Anesth Analg 2013; 116: 677–84 [PubMed: 22543064]

125. Carvalho AR, Bergamini BC, Carvalho NS, Cagido VR, Neto AC, Jandre FC, Zin WA, Giannella-Neto A: Volume-independent elastance: a useful parameter for open-lung positive end-expiratory pressure adjustment. Anesth Analg 2013; 116: 627–633 [PubMed: 22467900]

126. D'Antini D, Huhle R, Herrmann J, Sulemanji DS, Oto J, Raimondo P, Mirabella L, Hemmes SNT, Schultz MJ, Pelosi P, Kaczka DW, Vidal Melo MF, Gama de Abreu M, Cinnella G, European Society of A, the PVN: Respiratory System Mechanics During Low Versus High Positive End-Expiratory Pressure in Open Abdominal Surgery: A Substudy of PROVHILO Randomized Controlled Trial. Anesth Analg 2018; 126: 143–149 [PubMed: 28632529]

127. Carvalho AR, Spieth PM, Pelosi P, Vidal Melo MF, Koch T, Jandre FC, Giannella-Neto A, de Abreu MG: Ability of dynamic airway pressure curve profile and elastance for positive end-expiratory pressure titration. Intensive Care Med 2008; 34: 2291–9 [PubMed: 18825365]

128. Zannin E, Dellaca RL, Kostic P, Pompilio PP, Larsson A, Pedotti A, Hedenstierna G, Frykholm P: Optimizing positive end-expiratory pressure by oscillatory mechanics minimizes tidal recruitment and distension: an experimental study in a lavage model of lung injury. Crit Care 2012; 16: R217 [PubMed: 23134702]

129. Dellacà RL, Zannin E, Kostic P, Olerud MA, Pompilio PP, Hedenstierna G, Pedotti A, Frykholm P: Optimisation of positive end-expiratory pressure by forced oscillation technique in a lavage model of acute lung injury. Intensive Care Med 2011; 37: 1021–1030 [PubMed: 21455750]

130. Cressoni M, Chiurazzi C, Gotti M, Amini M, Brioni M, Algieri I, Cammaroto A, Rovati C, Massari D, di Castiglione CB, Nikolla K, Montaruli C, Lazzerini M, Dondossola D, Colombo A, Gatti S, Valerio V, Gagliano N, Carlesso E, Gattinoni L: Lung Inhomogeneities and Time Course of Ventilator-induced Mechanical Injuries. Anesthesiology 2015

131. Taguchi K: Energy-sensitive photon counting detector-based X-ray computed tomography. Radiological Physics and Technology 2017; 10: 8–22 [PubMed: 28138947]

132. Cereda M, Xin Y, Meeder N, Zeng J, Jiang Y, Hamedani H, Profka H, Kadlecek S, Clapp J, Deshpande CG, Wu J, Gee JC, Kavanagh BP, Rizi RR: Visualizing the Propagation of Acute Lung Injury. Anesthesiology 2016; 124: 121–31 [PubMed: 26536308]

133. Galban CJ, Han MK, Boes JL, Chughtai KA, Meyer CR, Johnson TD, Galban S, Rehemtulla A, Kazerooni EA, Martinez FJ, Ross BD: Computed tomography-based biomarker provides unique signature for diagnosis of COPD phenotypes and disease progression. Nat Med 2012; 18: 1711–5 [PubMed: 23042237]

134. Xin Y, Cereda M, Hamedani H, Pourfathi M, Siddiqui S, Meeder N, Kadlecek S, Duncan I, Profka H, Rajaei J, Tustison NJ, Gee JC, Kavanagh BP, Rizi RR: Unstable Inflation Causing Injury: Insight from Prone Position and Paired CT Scans. Am J Respir Crit Care Med 2018

135. Hoffman EA, Tajik JK, Kugelmass SD: Matching pulmonary structure and perfusion via combined dynamic multislice CT and thin-slice high-resolution CT. Comput Med Imaging Graph 1995; 19: 101–12 [PubMed: 7736410]

136. Pelosi P, de Abreu MG: Acute respiratory distress syndrome: we can't miss regional lung perfusion! BMC Anesthesiol 2015; 15: 35 [PubMed: 25792969]

137. Hoffman EA, Chon D: Computed tomography studies of lung ventilation and perfusion. Proc Am Thorac Soc 2005; 2: 492–8, 506 [PubMed: 16352755]

138. Dakin J, Jones AT, Hansell DM, Hoffman EA, Evans TW: Changes in lung composition and regional perfusion and tissue distribution in patients with ARDS. Respirology 2011; 16: 1265–72 [PubMed: 21883676]

139. Fernandez-Bustamante A, Easley RB, Fuld M, Mulreany D, Hoffman EA, Simon BA: Regional aeration and perfusion distribution in a sheep model of endotoxemic acute lung injury characterized by functional computed tomography imaging. Crit Care Med 2009; 37: 2402–2411 [PubMed: 19531954]

140. Richter T, Bellani G, Scott Harris R, Vidal Melo MF, Winkler T, Venegas JG, Musch G: Effect of prone position on regional shunt, aeration, and perfusion in experimental acute lung injury. Am J Respir Crit Care Med 2005; 172: 480–487 [PubMed: 15901611]

141. Easley RB, Fuld MK, Fernandez-Bustamante A, Hoffman EA, Simon BA: Mechanism of hypoxemia in acute lung injury evaluated by multidetector-row CT. Acad Radiol 2006; 13: 916–21 [PubMed: 16777566]

142. Chiumello D, Langer T, Vecchi V, Luoni S, Colombo A, Brioni M, Froio S, Cigada I, Coppola S, Protti A, Lazzerini M, Gattinoni L: Low-dose chest computed tomography for quantitative and visual anatomical analysis in patients with acute respiratory distress syndrome. Intensive Care Med 2014; 40: 691–9 [PubMed: 24647812]

143. Reske AW, Reske AP, Gast HA, Seiwerts M, Beda A, Gottschaldt U, Josten C, Schreiter D, Heller N, Wrigge H, Amato MB: Extrapolation from ten sections can make CT-based quantification of lung aeration more practicable. Intensive Care Med 2010; 36: 1836–1844 [PubMed: 20689909]

144. Beckmann U, Gillies DM, Berenholtz SM, Wu AW, Pronovost P: Incidents relating to the intra-hospital transfer of critically ill patients. An analysis of the reports submitted to the Australian Incident Monitoring Study in Intensive Care. Intensive Care Med 2004; 30: 1579–85 [PubMed: 14991102]

145. Schuster DP: Positron emission tomography: theory and its application to the study of lung disease. Am Rev Respir Dis 1989; 139: 818–40 [PubMed: 2647009]

146. Melroy S, Bauer C, McHugh M, Carden G, Stolin A, Majewski S, Brefczynski-Lewis J, Wuest T: Development and Design of Next-Generation Head-Mounted Ambulatory Microdose Positron-Emission Tomography (AM-PET) System. Sensors (Basel) 2017; 17

147. Koba W, Jelicks LA, Fine EJ: MicroPET/SPECT/CT imaging of small animal models of disease. Am J Pathol 2013; 182: 319–24 [PubMed: 23219729]

148. Mettler FA Jr., Huda W, Yoshizumi TT, Mahesh M: Effective doses in radiology and diagnostic nuclear medicine: a catalog. Radiology 2008; 248: 254–63 [PubMed: 18566177]

149. Dimastromatteo J, Charles EJ, Laubach VE: Molecular imaging of pulmonary diseases. Respir Res 2018; 19: 17 [PubMed: 29368614]

150. Chen DL, Schiebler ML, Goo JM, van Beek EJR: PET imaging approaches for inflammatory lung diseases: Current concepts and future directions. Eur J Radiol 2017; 86: 371–376 [PubMed: 27663638]

151. Richard JC, Le Bars D, Costes N, Bregeon F, Tourvieille C, Lavenne F, Janier M, Gimenez G, Guerin C: Alveolar recruitment assessed by positron emission tomography during experimental acute lung injury. Intensive Care Med 2006; 32: 1889–1894 [PubMed: 17047926]

152. Wellman TJ, Winkler T, Costa EL, Musch G, Harris RS, Venegas JG, Melo MF: Measurement of regional specific lung volume change using respiratory-gated PET of inhaled 13N-nitrogen. J Nucl Med 2010; 51: 646–53 [PubMed: 20237036]

153. Simon BA, Venegas JG: Analyzing 13NN lung washout curves in the presence of intraregional nonuniformities. J Appl Physiol (1985) 1994; 76: 956–64 [PubMed: 8175611]

154. Galletti GG, Venegas JG: Tracer kinetic model of regional pulmonary function using positron emission tomography. J Appl Physiol (1985) 2002; 93: 1104–14 [PubMed: 12183508]

155. O'Neill K, Venegas JG, Richter T, Harris RS, Layfield JD, Musch G, Winkler T, Melo MF: Modeling kinetics of infused 13NN-saline in acute lung injury. J Appl Physiol (1985) 2003; 95: 2471–84 [PubMed: 12897030]

156. Musch G, Harris RS, Vidal Melo MF, O'Neill KR, Layfield JD, Winkler T, Venegas JG: Mechanism by which a sustained inflation can worsen oxygenation in acute lung injury. Anesthesiology 2004; 100: 323–330 [PubMed: 14739807]

157. de Prost N, Tucci MR, Melo MF: Assessment of lung inflammation with 18F-FDG PET during acute lung injury. AJR Am J Roentgenol 2010; 195: 292–300 [PubMed: 20651183]

158. Hogg JC: Neutrophil kinetics and lung injury. Physiol Rev 1987; 67: 1249–95 [PubMed: 3317458]

159. McCall CE, Bass DA, Cousart S, DeChatelet LR: Enhancement of hexose uptake in human polymorphonuclear leukocytes by activated complement component C5a. Proc Natl Acad Sci U S A 1979; 76: 5896–900 [PubMed: 293691]

160. Zhou Z, Kozlowski J, Goodrich AL, Markman N, Chen DL, Schuster DP: Molecular imaging of lung glucose uptake after endotoxin in mice. Am J Physiol Lung Cell Mol Physiol 2005; 289: L760–8 [PubMed: 15980036]

161. Boellaard R: Standards for PET image acquisition and quantitative data analysis. J Nucl Med 2009; 50 Suppl 1: 11S–20S [PubMed: 19380405]

162. Patlak CS, Blasberg RG, Fenstermacher JD: Graphical evaluation of blood-to-brain transfer constants from multiple-time uptake data. J Cereb Blood Flow Metab 1983; 3: 1–7 [PubMed: 6822610]

163. Chen DL, Rosenbluth DB, Mintun MA, Schuster DP: FDG-PET imaging of pulmonary inflammation in healthy volunteers after airway instillation of endotoxin. J Appl Physiol (1985) 2006; 100: 1602–9 [PubMed: 16424067]

164. Jones HA, Sriskandan S, Peters AM, Pride NB, Krausz T, Boobis AR, Haslett C: Dissociation of neutrophil emigration and metabolic activity in lobar pneumonia and bronchiectasis. Eur Respir J 1997; 10: 795–803 [PubMed: 9150315]

165. Sokoloff L, Reivich M, Kennedy C, Des Rosiers MH, Patlak CS, Pettigrew KD, Sakurada O, Shinohara M: The [14C]deoxyglucose method for the measurement of local cerebral glucose utilization: theory, procedure, and normal values in the conscious and anesthetized albino rat. J Neurochem 1977; 28: 897–916 [PubMed: 864466]

166. Reivich M, Kuhl D, Wolf A, Greenberg J, Phelps M, Ido T, Casella V, Fowler J, Hoffman E, Alavi A, Som P, Sokoloff L: The [18F]fluorodeoxyglucose method for the measurement of local cerebral glucose utilization in man. Circ Res 1979; 44: 127–37 [PubMed: 363301]

167. Schroeder T, Vidal Melo MF, Musch G, Harris RS, Venegas JG, Winkler T: Modeling pulmonary kinetics of 2-deoxy-2-[18F]fluoro-D-glucose during acute lung injury. Acad Radiol 2008; 15: 763–75 [PubMed: 18486012]

168. Bellani G, Messa C, Guerra L, Spagnolli E, Foti G, Patroniti N, Fumagalli R, Musch G, Fazio F, Pesenti A: Lungs of patients with acute respiratory distress syndrome show diffuse inflammation in normally aerated regions: a [18F]-fluoro-2-deoxy-D-glucose PET/CT study. Crit Care Med 2009; 37: 2216–22 [PubMed: 19487931]

169. Tsuchida S, Engelberts D, Peltekova V, Hopkins N, Frndova H, Babyn P, McKerlie C, Post M, McLoughlin P, Kavanagh BP: Atelectasis causes alveolar injury in nonatelectatic lung regions. Am J Respir Crit Care Med 2006; 174: 279–289 [PubMed: 16675780]

170. Morais CCA, Koyama Y, Yoshida T, Plens GM, Gomes S, Lima C, Ramos OP, Pereira SM, Kawaguchi N, Yamamoto H, Uchiyama A, Borges JB, Vidal Melo MF, Tucci MR, Amato MBP, Kavanagh BP, Costa ELV, Fujino Y: High Positive End-Expiratory Pressure Renders Spontaneous Effort Non-Injurious. Am J Respir Crit Care Med 2018

171. Motta-Ribeiro GC, Hashimoto S, Winkler T, Baron RM, Grogg K, Paula L, Santos A, Zeng C, Hibbert K, Harris RS, Bajwa E, Vidal Melo MF: Deterioration of Regional Lung Strain and Inflammation during Early Lung Injury. Am J Respir Crit Care Med 2018

172. Katira BH, Kuebler WM, Kavanagh BP: Inspiratory preload obliteration may injure lungs via cyclical "on-off" vascular flow. Intensive Care Med 2018; 44: 1521–1523 [PubMed: 29270678]

173. Katira BH, Engelberts D, Otulakowski G, Giesinger RE, Yoshida T, Post M, Kuebler WM, Connelly KA, Kavanagh BP: Abrupt Deflation after Sustained Inflation Causes Lung Injury. Am J Respir Crit Care Med 2018

174. Baranga A, Appelt S, Romalis M, Erickson C, Young A, Cates G, Happer W: Polarization of 3He by Spin Exchange with Optically Pumped Rb and K Vapors. Phys Rev Lett 1998; 80: 2801–2804

175. Suchanek K, Cie lar K, Olejniczak Z, Pałasz T, Suchanek M, Dohnalik T: Hyperpolarized 3He gas production by metastability exchange optical pumping for magnetic resonance imaging. Optica Applicata 2005; 35: 263

176. Gast K, Eberle B, Schmiedeskamp J, Kauczor H-U: Magnetic resonance imaging using hyperpolarized 3He-gas. Acad Radiol 2003; 10: 1119–1131 [PubMed: 14587630]

177. Kadlecek S, Emami K, Fischer MC, Yu J, Ishii M, Lipson DA, Gefter WB, Shrager JB, Rizi RR: Imaging physiological parameters with hyperpolarized gas MRI. Progress In Nuclear Magnetic Resonance Spectroscopy 2005; 47: 187–212

178. Walker TG, Happer W: Spin-Exchange Optical Pumping of Noble-Gas Nuclei. Rev Mod Phys 1997; 69: 629–642

179. Siddiqui S, Kadlecek S, Pourfathi M, Xin Y, Mannherz W, Hamedani H, Drachman N, Ruppert K, Clapp J, Rizi R: The use of hyperpolarized carbon-13 magnetic resonance for molecular imaging. Adv Drug Deliv Rev 2017; 113: 3–23 [PubMed: 27599979]

180. Tusman G, Bohm SH, Tempra A, Melkun F, Garcia E, Turchetto E, Mulder PG, Lachmann B: Effects of recruitment maneuver on atelectasis in anesthetized children. Anesthesiology 2003; 98: 14–22 [PubMed: 12502973]

181. Eichinger M, Heussel CP, Kauczor HU, Tiddens H, Puderbach M: Computed tomography and magnetic resonance imaging in cystic fibrosis lung disease. J Magn Reson Imaging 2010; 32: 1370–8 [PubMed: 21105141]

182. Kauczor H-U, Ley-Zaporozhan J, Ley S: Imaging of Pulmonary Pathologies: Focus on Magnetic Resonance Imaging. Proceedings of the American Thoracic Society 2009; 6: 458–463 [PubMed: 19687219]

183. Sa RC, Henderson AC, Simonson T, Arai TJ, Wagner H, Theilmann RJ, Wagner PD, Prisk GK, Hopkins SR: Measurement of the distribution of ventilation-perfusion ratios in the human lung with proton MRI: comparison with the multiple inert-gas elimination technique. J Appl Physiol (1985) 2017; 123: 136–146 [PubMed: 28280105]

184. Prisk GK, Yamada K, Henderson AC, Arai TJ, Levin DL, Buxton RB, Hopkins SR: Pulmonary perfusion in the prone and supine postures in the normal human lung. J Appl Physiol 2007; 103: 883–894 [PubMed: 17569767]

185. Möller HE, Chen XJ, Saam B, Hagspiel KD, Johnson GA, Altes TA, Lange EEd, Kauczor H-U: MRI of the lungs using hyperpolarized noble gases. Magn Reson Med 2002; 47: 1029–1051 [PubMed: 12111949]

186. Fischer MC, Kadlecek S, Yu J, Ishii M, Emami K, Vahdat V, Lipson DA, Rizi RR: Measurements of regional alveolar oxygen pressure using hyperpolarized 3He MRI. Acad Radiol 2005; 12: 1430–1439 [PubMed: 16253855]

187. Woods JC, Choong CK, Yablonskiy DA, Bentley J, Wong J, Pierce JA, Cooper JD, Macklem PT, Conradi MS, Hogg JC: Hyperpolarized 3He diffusion MRI and histology in pulmonary emphysema. Magn Reson Med 2006; 56: 1293–1300 [PubMed: 17058206]

188. Yablonskiy DA, Sukstanskii AL, Leawoods JC, Gierada DS, Bretthorst GL, Lefrak SS, Cooper JD, Conradi MS: Quantitative in vivo assessment of lung microstructure at the alveolar level with hyperpolarized 3He diffusion MRI. Proc Natl Acad Sci 2002; 99: 3111–3116 [PubMed: 11867733]

189. Mansson S, Deninger AJ, Magnusson P, Pettersson G, Olsson LE, Hansson G, Wollmer P, Golman K: 3He MRI-based assessment of posture-dependent regional ventilation gradients in rats. J Appl Physiol 2005; 98: 2259–2267 [PubMed: 15640396]

190. Thomas AC, Nouls JC, Driehuys B, Voltz JW, Fubara B, Foley J, Bradbury JA, Zeldin DC: Ventilation defects observed with hyperpolarized 3He magnetic resonance imaging in a mouse model of acute lung injury. Am J Respir Cell Mol Biol 2011; 44: 648–654 [PubMed: 20595465]

191. Cereda M, Xin Y, Emami K, Huang J, Rajaei J, Profka H, Han B, Mongkolwisetwara P, Kadlecek S, Kuzma NN, Pickup S, Kavanagh BP, Deutschman CS, Rizi RR: Positive end-expiratory pressure increments during anesthesia in normal lung result in hysteresis and greater numbers of smaller aerated airspaces. Anesthesiology 2013; 119: 1402–9 [PubMed: 24025616]

192. Bachofen H, Gehr P, Weibel ER: Alterations of mechanical properties and morphology in excised rabbit lungs rinsed with a detergent. J Appl Physiol 1979; 47: 1002–1010 [PubMed: 511700]

193. Cereda M, Xin Y, Hamedani H, Clapp J, Kadlecek S, Meeder N, Zeng J, Profka H, Kavanagh BP, Rizi RR: Mild loss of lung aeration augments stretch in healthy lung regions. J Appl Physiol (1985) 2016; 120: 444–54 [PubMed: 26662053]

194. Ruppert K, Altes TA, Mata JF, Ruset IC, Hersman FW, Mugler JP: Detecting pulmonary capillary blood pulsations using hyperpolarized xenon-129 chemical shift saturation recovery (CSSR) MR spectroscopy. Magn Reson Med 2016; 75: 1771–1780 [PubMed: 26017009]

195. Victorino JA, Borges JB, Okamoto VN, Matos GF, Tucci MR, Caramez MP, Tanaka H, Sipmann FS, Santos DC, Barbas CS, Carvalho CR, Amato MB: Imbalances in regional lung ventilation: a validation study on electrical impedance tomography. Am J Respir Crit Care Med 2004; 169: 791–800 [PubMed: 14693669]

196. Frerichs I, Dargaville PA, van Genderingen H, Morel DR, Rimensberger PC: Lung volume recruitment after surfactant administration modifies spatial distribution of ventilation. Am J Respir Crit Care Med 2006; 174: 772–9 [PubMed: 16840739]

197. Blankman P, Hasan D, Erik G, Gommers D: Detection of 'best' positive end-expiratory pressure derived from electrical impedance tomography parameters during a decremental positive end-expiratory pressure trial. Crit Care 2014; 18: R95 [PubMed: 24887391]

198. Yoshida T, Engelberts D, Otulakowski G, Katira B, Post M, Ferguson ND, Brochard L, Amato MBP, Kavanagh BP: Continuous Negative Abdominal Pressure Reduces Ventilator-induced Lung Injury in a Porcine Model. Anesthesiology 2018

199. Yoshida T, Torsani V, Gomes S, De Santis RR, Beraldo MA, Costa EL, Tucci MR, Zin WA, Kavanagh BP, Amato MB: Spontaneous effort causes occult pendelluft during mechanical ventilation. Am J Respir Crit Care Med 2013; 188: 1420–7 [PubMed: 24199628]

200. Bellani G, Messa C, Guerra L, Spagnolli E, Foti G, Patroniti N, Fumagalli R, Musch G, Fazio F, Pesenti A: Lungs of patients with acute respiratory distress syndrome show diffuse inflammation in normally aerated regions: a [18F]-fluoro-2-deoxy-D-glucose PET/CT study. Crit Care Med 2009; 37: 2216–2222 [PubMed: 19487931]

201. Papazian L, Forel JM, Gacouin A, Penot-Ragon C, Perrin G, Loundou A, Jaber S, Arnal JM, Perez D, Seghboyan JM, Constantin JM, Courant P, Lefrant JY, Guerin C, Prat G, Morange S, Roch A, Investigators AS: Neuromuscular blockers in early acute respiratory distress syndrome. N Engl J Med 2010; 363: 1107–1116 [PubMed: 20843245]

202. Kendall JL, Hoffenberg SR, Smith RS: History of emergency and critical care ultrasound: the evolution of a new imaging paradigm. Crit Care Med 2007; 35: S126–130 [PubMed: 17446770]

203. Bertrand PB, Levine RA, Isselbacher EM, Vandervoort PM: Fact or Artifact in Two-Dimensional Echocardiography: Avoiding Misdiagnosis and Missed Diagnosis. J Am Soc Echocardiogr 2016; 29: 381–391 [PubMed: 26969139]

204. Aldrich JE: Basic physics of ultrasound imaging. Crit Care Med 2007; 35: S131–137 [PubMed: 17446771]

205. Edelman SK: Understanding ultrasound physics, Baker & Taylor, 2003

206. Feldman MK, Katyal S, Blackwood MS: US artifacts. Radiographics: A Review Publication of the Radiological Society of North America, Inc 2009; 29: 1179–1189

207. Soldati G, Demi M: The use of lung ultrasound images for the differential diagnosis of pulmonary and cardiac interstitial pathology. J Ultrasound 2017; 20: 91–96 [PubMed: 28592998]

208. Soldati G, Demi M, Inchingolo R, Smargiassi A, Demi L: On the Physical Basis of Pulmonary Sonographic Interstitial Syndrome. J Ultrasound Med 2016; 35: 2075–86 [PubMed: 27503755]

209. Downie JM, Nam AJ, Simon BA: Pressure-volume curve does not predict steady-state lung volume in canine lavage lung injury. Am J Respir Crit Care Med 2004; 169: 957–962 [PubMed: 14764430]

210. Lichtenstein DA, Mezière GA: Relevance of lung ultrasound in the diagnosis of acute respiratory failure: the BLUE protocol. Chest 2008; 134: 117–125 [PubMed: 18403664]

211. Lichtenstein D, Meziere G, Biderman P, Gepner A, Barre O: The comet-tail artifact. An ultrasound sign of alveolar-interstitial syndrome. Am J Respir Crit Care Med 1997; 156: 1640–6 [PubMed: 9372688]

212. Volpicelli G: Lung sonography. J Ultrasound Med 2013; 32: 165–171 [PubMed: 23269722]

213. Pivetta E, Baldassa F, Masellis S, Bovaro F, Lupia E, Maule MM: Sources of Variability in the Detection of B-Lines, Using Lung Ultrasound. Ultrasound Med Biol 2018; 44: 1212–1216 [PubMed: 29598962]

214. Alrajab S, Youssef AM, Akkus NI, Caldito G: Pleural ultrasonography versus chest radiography for the diagnosis of pneumothorax: review of the literature and meta-analysis. Crit Care 2013; 17: R208 [PubMed: 24060427]

215. Enriquez JL, Wu TS: An introduction to ultrasound equipment and knobology. Crit Care Clin 2014; 30: 25–45, v [PubMed: 24295840]

216. Xirouchaki N, Kondili E, Prinianakis G, Malliotakis P, Georgopoulos D: Impact of lung ultrasound on clinical decision making in critically ill patients. Intensive Care Med 2014; 40: 57–65 [PubMed: 24158410]

217. Nazerian P, Volpicelli G, Vanni S, Gigli C, Betti L, Bartolucci M, Zanobetti M, Ermini FR, Iannello C, Grifoni S: Accuracy of lung ultrasound for the diagnosis of consolidations when compared to chest computed tomography. Am J Emerg Med 2015; 33: 620–5 [PubMed: 25758182]

218. Alzahrani SA, Al-Salamah MA, Al-Madani WH, Elbarbary MA: Systematic review and meta-analysis for the use of ultrasound versus radiology in diagnosing of pneumonia. Crit Ultrasound J 2017; 9: 6 [PubMed: 28244009]

219. Ye X, Xiao H, Chen B, Zhang S: Accuracy of Lung Ultrasonography versus Chest Radiography for the Diagnosis of Adult Community-Acquired Pneumonia: Review of the Literature and Meta-Analysis. PLoS One 2015; 10: e0130066 [PubMed: 26107512]

220. Reissig A, Copetti R, Mathis G, Mempel C, Schuler A, Zechner P, Aliberti S, Neumann R, Kroegel C, Hoyer H: Lung ultrasound in the diagnosis and follow-up of community-acquired pneumonia: a prospective, multicenter, diagnostic accuracy study. Chest 2012; 142: 965–972 [PubMed: 22700780]

221. Martindale JL, Secko M, Kilpatrick JF, deSouza IS, Paladino L, Aherne A, Mehta N, Conigiliaro A, Sinert R: Serial Sonographic Assessment of Pulmonary Edema in Patients With Hypertensive Acute Heart Failure. J Ultrasound Med 2018; 37: 337–345 [PubMed: 28758715]

222. Jiang L, Ma Y, Zhao C, Shen W, Feng X, Xu Y, Zhang M: Role of Transthoracic Lung Ultrasonography in the Diagnosis of Pulmonary Embolism: A Systematic Review and Meta-Analysis. PloS One 2015; 10: e0129909 [PubMed: 26076021]

223. Squizzato A, Rancan E, Dentali F, Bonzini M, Guasti L, Steidl L, Mathis G, Ageno W: Diagnostic accuracy of lung ultrasound for pulmonary embolism: a systematic review and meta-analysis. J Thromb Haemost 2013; 11: 1269–78 [PubMed: 23574640]

224. Winkler MH, Touw HR, van de Ven PM, Twisk J, Tuinman PR: Diagnostic Accuracy of Chest Radiograph, and When Concomitantly Studied Lung Ultrasound, in Critically Ill Patients With Respiratory Symptoms: A Systematic Review and Meta-Analysis. Crit Care Med 2018; 46: e707–e714 [PubMed: 29601314]

225. Soldati G, Testa A, Silva FR, Carbone L, Portale G, Silveri NG: Chest ultrasonography in lung contusion. Chest 2006; 130: 533–8 [PubMed: 16899855]

226. Song G, Bae SC, Lee YH: Diagnostic accuracy of lung ultrasound for interstitial lung disease in patients with connective tissue diseases: a meta-analysis. Clin Exp Rheumatol 2016; 34: 11–6 [PubMed: 26812366]

227. Yousefifard M, Baikpour M, Ghelichkhani P, Asady H, Shahsavari Nia K, Moghadas Jafari A, Hosseini M, Safari S: Screening Performance Characteristic of Ultrasonography and Radiography in Detection of Pleural Effusion; a Meta-Analysis. Emerg (Tehran) 2016; 4: 1–10 [PubMed: 26862542]

228. Peris A, Tutino L, Zagli G, Batacchi S, Cianchi G, Spina R, Bonizzoli M, Migliaccio L, Perretta L, Bartolini M, Ban K, Balik M: The use of point-of-care bedside lung ultrasound significantly reduces the number of radiographs and computed tomography scans in critically ill patients. Anesth Analg 2010; 111: 687–92 [PubMed: 20733164]

229. Chiumello D, Mongodi S, Algieri I, Vergani GL, Orlando A, Via G, Crimella F, Cressoni M, Mojoli F: Assessment of Lung Aeration and Recruitment by CT Scan and Ultrasound in Acute Respiratory Distress Syndrome Patients. Crit Care Med 2018

230. Bouhemad B, Brisson H, Le-Guen M, Arbelot C, Lu Q, Rouby J-J: Bedside ultrasound assessment of positive end-expiratory pressure-induced lung recruitment. Am J Respir Crit Care Med 2011; 183: 341–347 [PubMed: 20851923]

231. Haddam M, Zieleskiewicz L, Perbet S, Baldovini A, Guervilly C, Arbelot C, Noel A, Vigne C, Hammad E, Antonini F, Lehingue S, Peytel E, Lu Q, Bouhemad B, Golmard JL, Langeron O, Martin C, Muller L, Rouby JJ, Constantin JM, Papazian L, Leone M, Network CAEC, AzuRea Collaborative N: Lung ultrasonography for assessment of oxygenation response to prone position ventilation in ARDS. Intensive Care Med 2016; 42: 1546–1556 [PubMed: 27324241]

232. Pichette M, Goffi A: A 45-Year-Old Man With Severe Respiratory Failure After Cardiac Arrest. Chest 2018; 153: e133–e137 [PubMed: 29884275]

233. Prat G, Guinard S, Bizien N, Nowak E, Tonnelier JM, Alavi Z, Renault A, Boles JM, L'Her E: Can lung ultrasonography predict prone positioning response in acute respiratory distress syndrome patients? J Crit Care 2016; 32: 36–41 [PubMed: 26806842]

234. Song I-K, Kim E- H, Lee J- H, Ro S, Kim H- S, Kim J- T: Effects of an alveolar recruitment manoeuvre guided by lung ultrasound on anaesthesia-induced atelectasis in infants: a randomised, controlled trial. Anaesthesia 2017; 72: 214–222 [PubMed: 27804117]

235. Stefanidis K, Dimopoulos S, Tripodaki ES, Vitzilaios K, Politis P, Piperopoulos P, Nanas S: Lung sonography and recruitment in patients with early acute respiratory distress syndrome: a pilot study. Crit Care 2011; 15: R185 [PubMed: 21816054]

236. Tusman G, Acosta CM, Costantini M: Ultrasonography for the assessment of lung recruitment maneuvers. Crit Ultrasound J 2016; 8: 8 [PubMed: 27496127]

237. Mongodi S, Pozzi M, Orlando A, Bouhemad B, Stella A, Tavazzi G, Via G, Iotti GA, Mojoli F: Lung ultrasound for daily monitoring of ARDS patients on extracorporeal membrane oxygenation: preliminary experience. Intensive Care Med 2018; 44: 123–124 [PubMed: 28936711]

238. Tusman G, Acosta CM, Nicola M, Esperatti M, Bohm SH, Suarez-Sipmann F: Real-time images of tidal recruitment using lung ultrasound. Crit Ultrasound J 2015; 7: 19 [PubMed: 26660526]

239. Wang XT, Ding X, Zhang HM, Chen H, Su LX, Liu DW, Chinese Critical Ultrasound Study G: Lung ultrasound can be used to predict the potential of prone positioning and assess prognosis in patients with acute respiratory distress syndrome. Crit Care 2016; 20: 385 [PubMed: 27899151]

240. Bouhemad B, Brisson H, Le-Guen M, Arbelot C, Lu Q, Rouby JJ: Bedside ultrasound assessment of positive end-expiratory pressure-induced lung recruitment. Am J Respir Crit Care Med 2011; 183: 341–7 [PubMed: 20851923]

241. Soummer A, Perbet S, Brisson H, Arbelot C, Constantin JM, Lu Q, Rouby JJ, Lung Ultrasound Study G: Ultrasound assessment of lung aeration loss during a successful weaning trial predicts postextubation distress*. Crit Care Med 2012; 40: 2064–72 [PubMed: 22584759]

242. Silva S, Ait Aissa D, Cocquet P, Hoarau L, Ruiz J, Ferre F, Rousset D, Mora M, Mari A, Fourcade O, Riu B, Jaber S, Bataille B: Combined Thoracic Ultrasound Assessment during a Successful Weaning Trial Predicts Postextubation Distress. Anesthesiology 2017; 127: 666–674 [PubMed: 28650414]

243. Gargani L, Lionetti V, Di Cristofano C, Bevilacqua G, Recchia FA, Picano E: Early detection of acute lung injury uncoupled to hypoxemia in pigs using ultrasound lung comets. Crit Care Med 2007; 35: 2769–74 [PubMed: 17828031]

244. Shen P, Zong Y-m, Shu J, Shi Y-c, Zhu W-j, Qian H-j, Yang M-x, Zhang M: Dynamic assessment of lung injury by ultrasound in a case with H7N9 influenza. Crit Care 2013; 17: 438 [PubMed: 23805783]

245. Testa A, Soldati G, Copetti R, Giannuzzi R, Portale G, Gentiloni-Silveri N: Early recognition of the 2009 pandemic influenza A (H1N1) pneumonia by chest ultrasound. Crit Care 2012; 16: R30 [PubMed: 22340202]

246. Tardella M, Gutierrez M, Salaffi F, Carotti M, Ariani A, Bertolazzi C, Filippucci E, Grassi W: Ultrasound in the assessment of pulmonary fibrosis in connective tissue disorders: correlation with high-resolution computed tomography. J Rheumatol 2012; 39: 1641–1647 [PubMed: 22753655]

247. Via G, Lichtenstein D, Mojoli F, Rodi G, Neri L, Storti E, Klersy C, Iotti G, Braschi A: Whole lung lavage: a unique model for ultrasound assessment of lung aeration changes. Intensive Care Med 2010; 36: 999–1007 [PubMed: 20221746]

248. Soldati G, Inchingolo R, Smargiassi A, Sher S, Nenna R, Inchingolo CD, Valente S: Ex vivo lung sonography: morphologic-ultrasound relationship. Ultrasound in Medicine & Biology 2012; 38: 1169–1179 [PubMed: 22579543]

249. Enghard P, Rademacher S, Nee J, Hasper D, Engert U, Jörres A, Kruse JM: Simplified lung ultrasound protocol shows excellent prediction of extravascular lung water in ventilated intensive care patients. Crit Care 2015; 19: 36 [PubMed: 25656060]

250. Jambrik Z, Monti S, Coppola V, Agricola E, Mottola G, Miniati M, Picano E: Usefulness of ultrasound lung comets as a nonradiologic sign of extravascular lung water. Am J Cardiol 2004; 93: 1265–1270 [PubMed: 15135701]

251. Lichtenstein D, Mézière G, Biderman P, Gepner A, Barré O: The comet-tail artifact. An ultrasound sign of alveolar-interstitial syndrome. Am J Respir Crit Care Med 1997; 156: 1640–1646 [PubMed: 9372688]

252. Volpicelli G, Skurzak S, Boero E, Carpinteri G, Tengattini M, Stefanone V, Luberto L, Anile A, Cerutti E, Radeschi G, Frascisco MF: Lung ultrasound predicts well extravascular lung water but is of limited usefulness in the prediction of wedge pressure. Anesthesiology 2014; 121: 320–327 [PubMed: 24821071]

253. Anderson KL, Fields JM, Panebianco NL, Jenq KY, Marin J, Dean AJ: Inter-rater reliability of quantifying pleural B-lines using multiple counting methods. J Ultrasound Med 2013; 32: 115–120 [PubMed: 23269716]

254. Bedetti G, Gargani L, Corbisiero A, Frassi F, Poggianti E, Mottola G: Evaluation of ultrasound lung comets by hand-held echocardiography. Cardiovascular Ultrasound 2006; 4: 34 [PubMed: 16945139]

255. Cardinale L, Volpicelli G, Binello F, Garofalo G, Priola SM, Veltri A, Fava C: Clinical application of lung ultrasound in patients with acute dyspnea: differential diagnosis between cardiogenic and pulmonary causes. La Radiologia Medica 2009; 114: 1053–1064 [PubMed: 19697100]

256. Liteplo AS, Marill KA, Villen T, Miller RM, Murray AF, Croft PE, Capp R, Noble VE: Emergency thoracic ultrasound in the differentiation of the etiology of shortness of breath (ETUDES): sonographic B-lines and N-terminal pro-brain-type natriuretic peptide in diagnosing congestive heart failure. Acad Emerg Med 2009; 16: 201–210 [PubMed: 19183402]

257. Al Deeb M, Barbic S, Featherstone R, Dankoff J, Barbic D: Point-of-care ultrasonography for the diagnosis of acute cardiogenic pulmonary edema in patients presenting with acute dyspnea: a systematic review and meta-analysis. Acad Emerg Med 2014; 21: 843–852 [PubMed: 25176151]

258. Cibinel GA, Casoli G, Elia F, Padoan M, Pivetta E, Lupia E, Goffi A: Diagnostic accuracy and reproducibility of pleural and lung ultrasound in discriminating cardiogenic causes of acute dyspnea in the emergency department. Internal and Emergency Medicine 2012; 7: 65–70 [PubMed: 22033792]

259. Pivetta E, Goffi A, Lupia E, Tizzani M, Porrino G, Ferreri E, Volpicelli G, Balzaretti P, Banderali A, Iacobucci A, Locatelli S, Casoli G, Stone MB, Maule MM, Baldi I, Merletti F, Cibinel GA, Baron P, Battista S, Buonafede G, Busso V, Conterno A, Del Rizzo P, Ferrera P, Pecetto PF, Moiraghi C, Morello F, Steri F, Ciccone G, Calasso C, Caserta MA, Civita M, Condo' C, D'Alessandro V, Del Colle S, Ferrero S, Griot G, Laurita E, Lazzero A, Lo Curto F, Michelazzo M, Nicosia V, Palmari N, Ricchiardi A, Rolfo A, Rostagno R, Bar F, Boero E, Frascisco M, Micossi I, Mussa A, Stefanone V, Agricola R, Cordero G, Corradi F, Runzo C, Soragna A, Sciullo D, Vercillo D, Allione A, Artana N, Corsini F, Dutto L, Lauria G, Morgillo T, Tartaglino B, Bergandi D, Cassetta I, Masera C, Garrone M, Ghiselli G, Ausiello L, Barutta L, Bernardi E, Bono A, Forno D, Lamorte A, Lison D, Lorenzati B, Maggio E, Masi I, Maggiorotto M, Novelli G, Panero F, Perotto M, Ravazzoli M, Saglio E, Soardo F, Tizzani A, Tizzani P, Tullio M, Ulla M, Romagnoli E, Piedmont SGfLUitEDi: Lung Ultrasound-Implemented Diagnosis of Acute Decompensated Heart Failure in the ED: A SIMEU Multicenter Study. Chest 2015; 148: 202–210 [PubMed: 25654562]

260. Volpicelli G, Mussa A, Garofalo G, Cardinale L, Casoli G, Perotto F, Fava C, Frascisco M: Bedside lung ultrasound in the assessment of alveolar-interstitial syndrome. Am J Emerg Med 2006; 24: 689–696 [PubMed: 16984837]

261. Platz E, Lewis EF, Uno H, Peck J, Pivetta E, Merz AA, Hempel D, Wilson C, Frasure SE, Jhund PS, Cheng S, Solomon SD: Detection and prognostic value of pulmonary congestion by lung

ultrasound in ambulatory heart failure patients. Eur Heart J 2016; 37: 1244–1251 [PubMed: 26819225]

262. Zoccali C, Torino C, Tripepi R, Tripepi G, D'Arrigo G, Postorino M, Gargani L, Sicari R, Picano E, Mallamaci F, Group LUiCW: Pulmonary congestion predicts cardiac events and mortality in ESRD. Journal of the American Society of Nephrology: JASN 2013; 24: 639–646 [PubMed: 23449536]

263. Sekiguchi H, Schenck LA, Horie R, Suzuki J, Lee EH, McMenomy BP, Chen TE, Lekah A, Mankad SV, Gajic O: Critical care ultrasonography differentiates ARDS, pulmonary edema, and other causes in the early course of acute hypoxemic respiratory failure. Chest 2015; 148: 912–918 [PubMed: 25996139]

264. Riviello ED, Kiviri W, Twagirumugabe T, Mueller A, Banner-Goodspeed VM, Officer L, Novack V, Mutumwinka M, Talmor DS, Fowler RA: Hospital Incidence and Outcomes of the Acute Respiratory Distress Syndrome Using the Kigali Modification of the Berlin Definition. Am J Respir Crit Care Med 2016; 193: 52–9 [PubMed: 26352116]

265. Vercesi V, Pisani L, van Tongeren PSI, Lagrand WK, Leopold SJ, Huson MMA, Henwood PC, Walden A, Smit M, Riviello ED, Pelosi P, Dondorp AM, Schultz MJ, Lung Ultrasound C: External confirmation and exploration of the Kigali modification for diagnosing moderate or severe ARDS. Intensive Care Med 2018; 44: 523–524 [PubMed: 29368056]

266. Copetti R, Soldati G, Copetti P: Chest sonography: a useful tool to differentiate acute cardiogenic pulmonary edema from acute respiratory distress syndrome. Cardiovasc Ultrasound 2008; 6: 16 [PubMed: 18442425]

267. Laursen CB, Sloth E, Lassen AT, Christensen Rd, Lambrechtsen J, Madsen PH, Henriksen DP, Davidsen JR, Rasmussen F: Point-of-care ultrasonography in patients admitted with respiratory symptoms: a single-blind, randomised controlled trial. Lancet Respir Med 2014; 2: 638–646 [PubMed: 24998674]

268. Rouby JJ, Arbelot C, Gao Y, Zhang M, Lv J, An Y, Wang C, Bin D, Barbas CSV, Dexheimer Neto FL, Prior Caltabeloti F, Lima E, Cebey A, Perbet S, Constantin JM, group As: Training for Lung Ultrasound Score Measurement in Critically Ill Patients. Am J Respir Crit Care Med 2018

269. See KC, Ong V, Wong SH, Leanda R, Santos J, Taculod J, Phua J, Teoh CM: Lung ultrasound training: curriculum implementation and learning trajectory among respiratory therapists. Intensive Care Med 2016; 42: 63–71 [PubMed: 26474994]

270. Brandli L: Benefits of protocol-driven ultrasound exams. Radiology Management 2007; 29: 56–59

271. Pian L, Gillman LM, McBeth PB, Xiao Z, Ball CG, Blaivas M, Hamilton DR, Kirkpatrick AW: Potential Use of Remote Telesonography as a Transformational Technology in Underresourced and/or Remote Settings. Emerg Med Int 2013; 2013: 986160 [PubMed: 23431455]

272. Corradi F, Brusasco C, Vezzani A, Santori G, Manca T, Ball L, Nicolini F, Gherli T, Brusasco V: Computer-Aided Quantitative Ultrasonography for Detection of Pulmonary Edema in Mechanically Ventilated Cardiac Surgery Patients. Chest 2016; 150: 640–51 [PubMed: 27130285]

273. Shankar H, Pagel PS: Potential adverse ultrasound-related biological effects: a critical review. Anesthesiology 2011; 115: 1109–24 [PubMed: 21866043]

274. Cao WJ, Rosenblat JD, Roth NC, Kuliszewski MA, Matkar PN, Rudenko D, Liao C, Lee PJH, Leong-Poi H: Therapeutic Angiogenesis by Ultrasound-Mediated MicroRNA-126-3p Delivery. Arteriosclerosis, Thrombosis, and Vascular Biology 2015; 35: 2401–2411

275. Fekri F, Delos Santos RC, Karshafian R, Antonescu CN: Ultrasound Microbubble Treatment Enhances Clathrin-Mediated Endocytosis and Fluid-Phase Uptake through Distinct Mechanisms. PloS One 2016; 11: e0156754 [PubMed: 27275866]

276. Sugiyama MG, Mintsopoulos V, Raheel H, Goldenberg NM, Batt JE, Brochard L, Kuebler WM, Leong-Poi H, Karshafian R, Lee WL: Lung Ultrasound and Microbubbles Enhance Aminoglycoside Efficacy and Delivery to the Lung in E. Coli-induced Pneumonia and ARDS. Am J Respir Crit Care Med 2018 doi: 10.1164/rccm.201711-2259LE [Epub ahead of print]
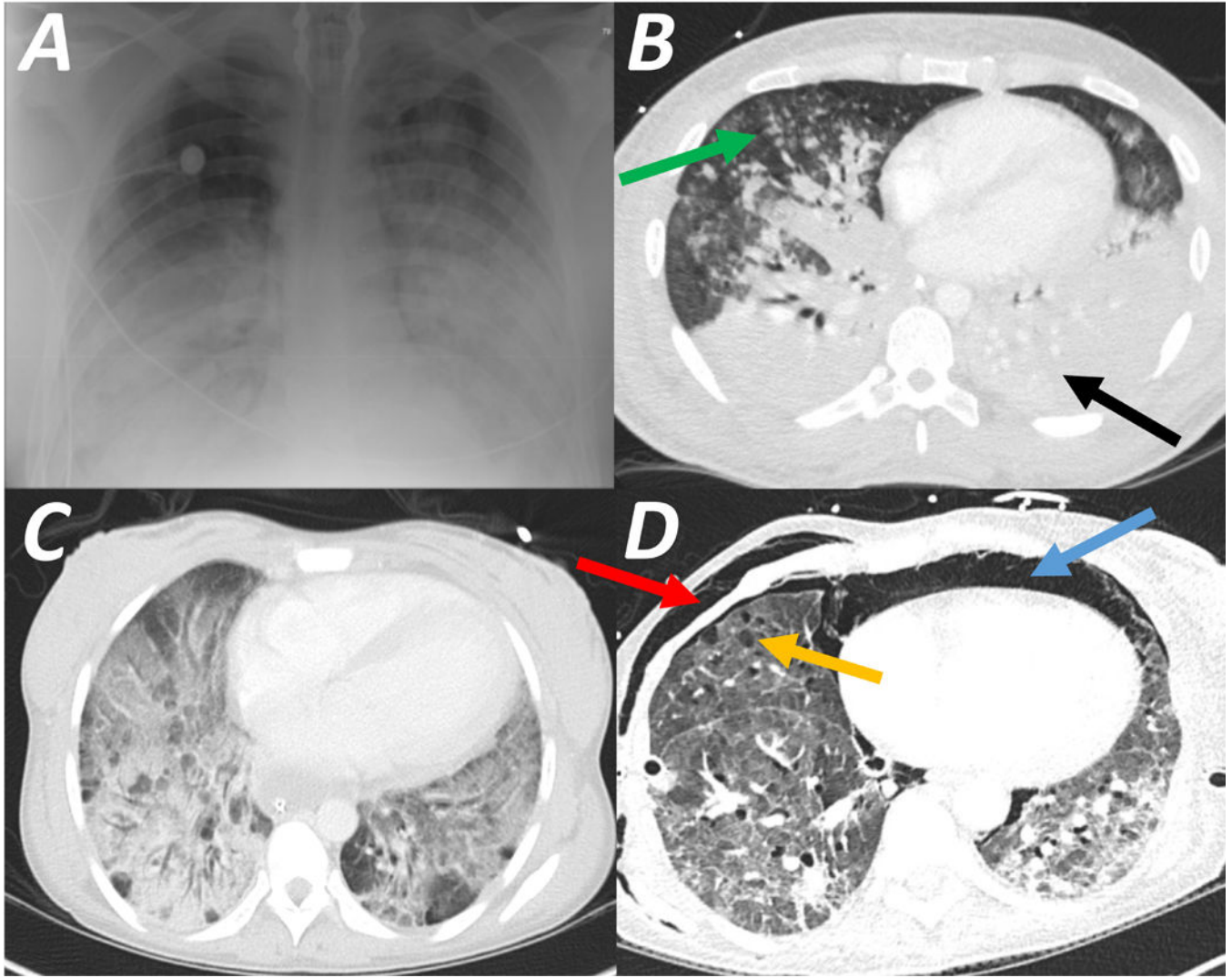
Summary statement:

'Pulmonary imaging provides major insights into the pathophysiology of lung injury and informs current respiratory care. Integrated approaches to conventional and advanced imaging, including bedside techniques, will continue to advance management of the injured lung.'
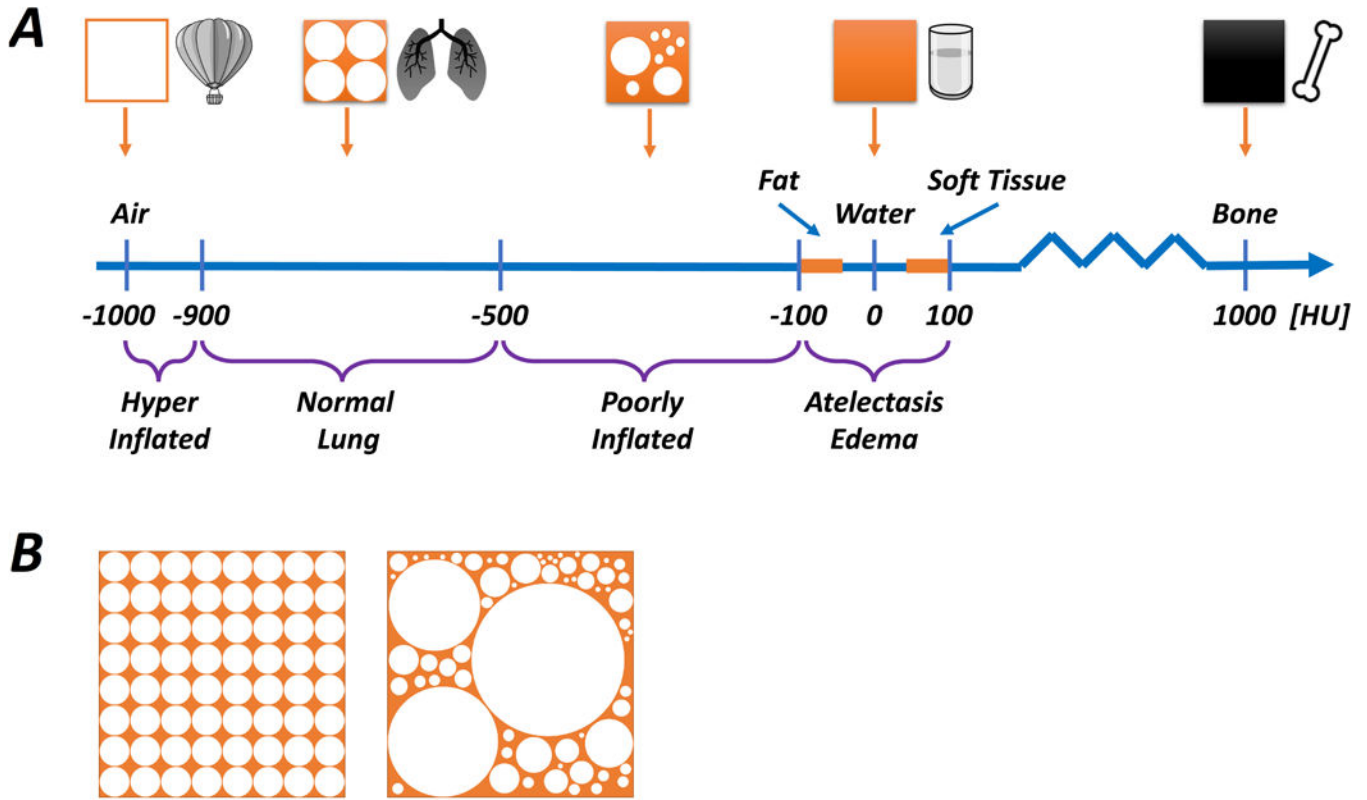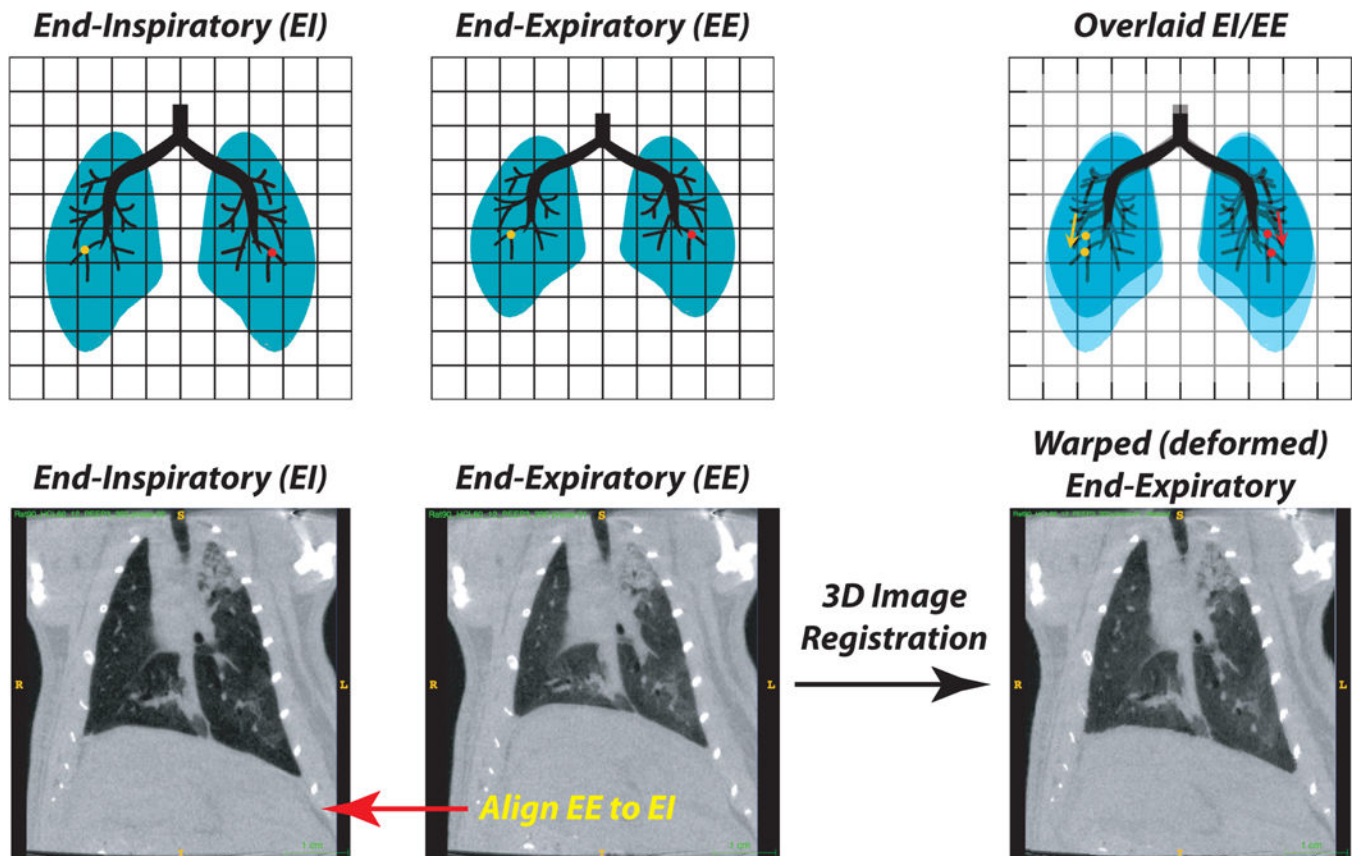
Figure 1:
Chest imaging in patients with Acute Respiratory Distress Syndrome (ARDS). Plain chest radiograph (*CXR, Panel A*) demonstrates symmetric widespread hazy infiltrates. In the same patient computed tomography scan (*CT, Panel B*) confirms the bilateral infiltration observed on plain CXR; however, the infiltrate is predominantly in the dorsal lung (black arrow), and the ventral lung regions are aerated ('baby lung', green arrow). *Panel C* is a CT scan showing typical ground glass opacities, indicating severely decreased aeration, but without complete loss of gas content. *Panel D* is a CT scan of a patient 16 days after the onset of ARDS, showing diffuse interstitial thickening predominantly at the lung bases, suggesting evolving fibrosis; in addition, ventral bullae (orange arrow), pneumomediastinum (blue arrow), and soft tissue emphysema (red arrow) represent barotrauma from mechanical ventilation.
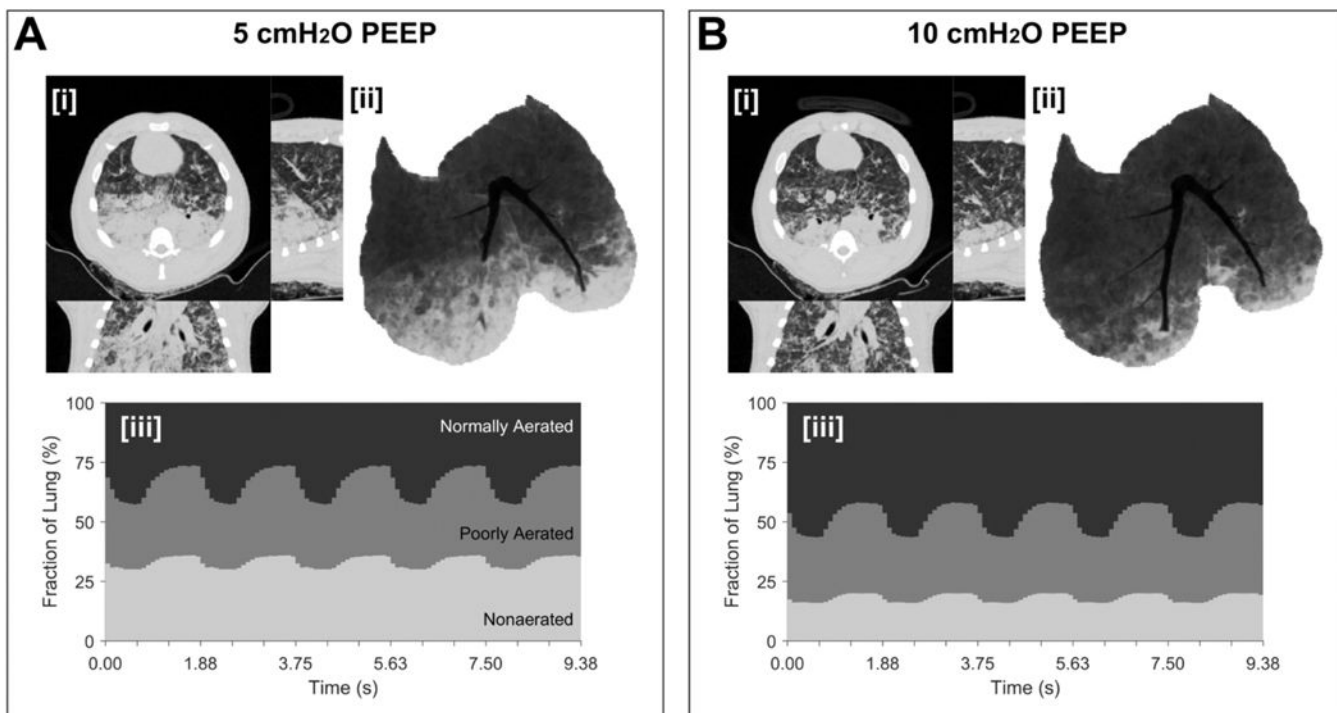
Figure 2:
Schematic illustration of CT densities relative to air, normal lung, water and bone (***Panel A***). The smallest unit of imaged tissue is called a voxel (≈ 1 mm^3), and the average density, expressed as Hounsfield Units (HU), of each voxel is determined by its contents. Higher density contents absorb more radiation and the image is whiter, whereas lower density contents absorb less radiation and the image is darker. If a voxel was composed *entirely* of air, water or bone it would have densities of -1000 HU, 0 HU and +700 HU, respectively. The density of fat, water and soft tissue are similar (fat   water   soft tissue), and normally aerated lung tissue (corresponding approximately to 50-70% air, 30-50% tissue) has a density of < -500 HU. Therefore, a hyperinflated region of lung (more air, less tissue) would have a density of far less than -500 HU (generally < -900 HU), whereas an area with substantial consolidation or atelectasis will have density of more than -100 HU. Areas with decreased (but not eliminated) aeration, called 'poorly aerated' lung, have density in the range of -500 to -100 HU. ***Panel B*** illustrates a range of possible content combinations within a single voxel. It is important to understand that the maximum resolution for CT is limited by the size of the voxel, and each voxel can only yield a single 'net' value for density. Thus, the illustrated voxels, while having different individual constitutions, each have a similar 'average' density expressed as HU.
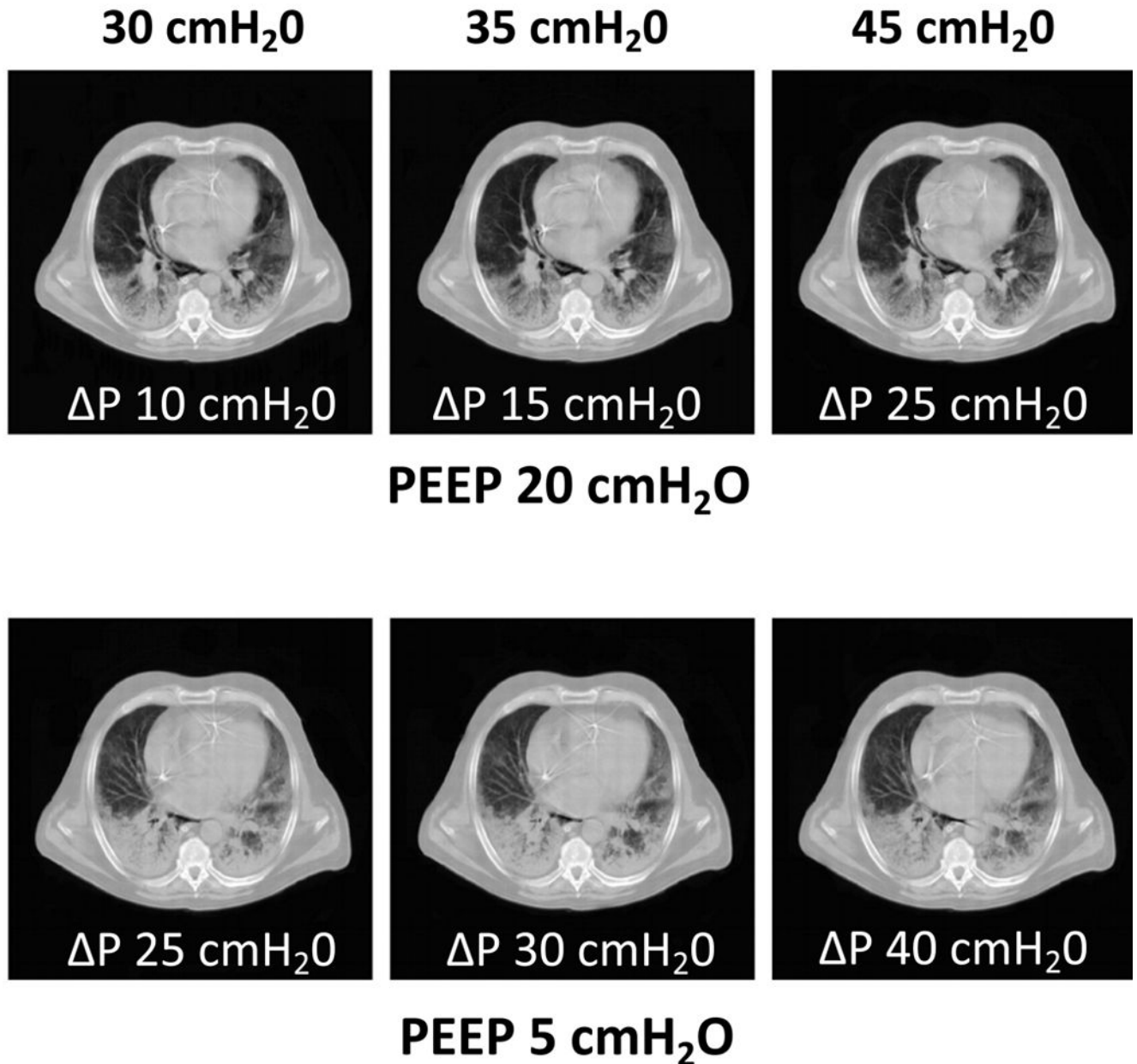
Figure 3:
Schematic showing the process of image registration between end-inspiratory (EI) and end-expiratory (EE) images (***Upper Panels*** *- Schematic;* ***Lower Panels -*** *representative CT slices*). The end-expiratory image is expanded in three dimensions to align all visible tissue features, including airways and blood vessels, to the target end-inspiratory image. With registration of tissue points, it is then possible to track the displacement that any point in the image undergoes during each tidal deflation (*e.g.*, the red and yellow dots). The product of the registration is thus a 'warped' (*i.e.* constrained fit) end-expiratory image. An example of image registration performed on end-inspiratory and end-expiratory CT scans obtained in a ventilated rat after lung injury is shown (***Bottom Panel***; see also *Supplemental Digital content* 1).

Figure 4:

Dynamic computed tomography (CT) illustrates the real-time spatial distribution of lung aeration during mechanical ventilation in experimental lung injury. Lung injury was induced by oleic acid infusion (see video - Supplemental Digital Content 2). Pressure-controlled ventilation (driving pressure 20 cmH$_2$O, rate 32 min–1, Inspired O$_2$ 40%) with lower PEEP (5 cmH$_2$O, *Panel A*) or higher PEEP (10 cmH$_2$O, *Panel B*) was used. In each panel, [i] end-inspiratory CT (transverse, sagittal, coronal planes), [ii] minimum intensity projection voxels, and [iii] time- varying fractions of lung at normally-aerated, poorly-aerated and non-aerated levels are illustrated. The following features are observed. Hyperaerated tissue (not visible) accounted for <1% of lung voxels at either level of PEEP. The intra-tidal changes in normal, poorly and non-aerated fraction were 15, 10 and 5%, respectively, at the two PEEP levels. However, there was a nearly two-fold increase in non-aerated tissue at the lower PEEP, as well as noticeable flooding of large bronchi in the right lung and arterial hemoglobin O$_2$ saturation was 92 *vs.* 63% with PEEP 10 *vs.* 5 cmH$_2$O. Normal, poor and non-aeration is considered: −900 to −500, −500 to −100, and above −100 HU, respectively.

Plateau Pressure

30 cmH$_2$0 35 cmH$_2$0 45 cmH$_2$0

ΔP 10 cmH$_2$0 ΔP 15 cmH$_2$0 ΔP 25 cmH$_2$0

PEEP 20 cmH$_2$O

ΔP 25 cmH$_2$0 ΔP 30 cmH$_2$0 ΔP 40 cmH$_2$0

PEEP 5 cmH$_2$O

Figure 5:
End-expiratory CT scans obtained in a patient with ARDS at high PEEP (20 cmH$_2$O, **Panel A**) and low PEEP (5 cmH$_2$O, **Panel B**). In each panel, three values of inspiratory plateau pressure (P$_{plat}$ 30, 35 and 45 cmH$_2$O) are targeted, and in each case the resultant driving pressure (P = P$_{plat}$ - PEEP) is indicated below each image. For each P$_{plat}$, atelectasis was more pronounced when the PEEP was lower, irrespective of the inspiratory P. The CT illustrates that alveolar recruitment achieved by high inflation pressure is not maintained

during expiration unless stabilized by sufficient PEEP. Reproduced with permission, Ref. 110.
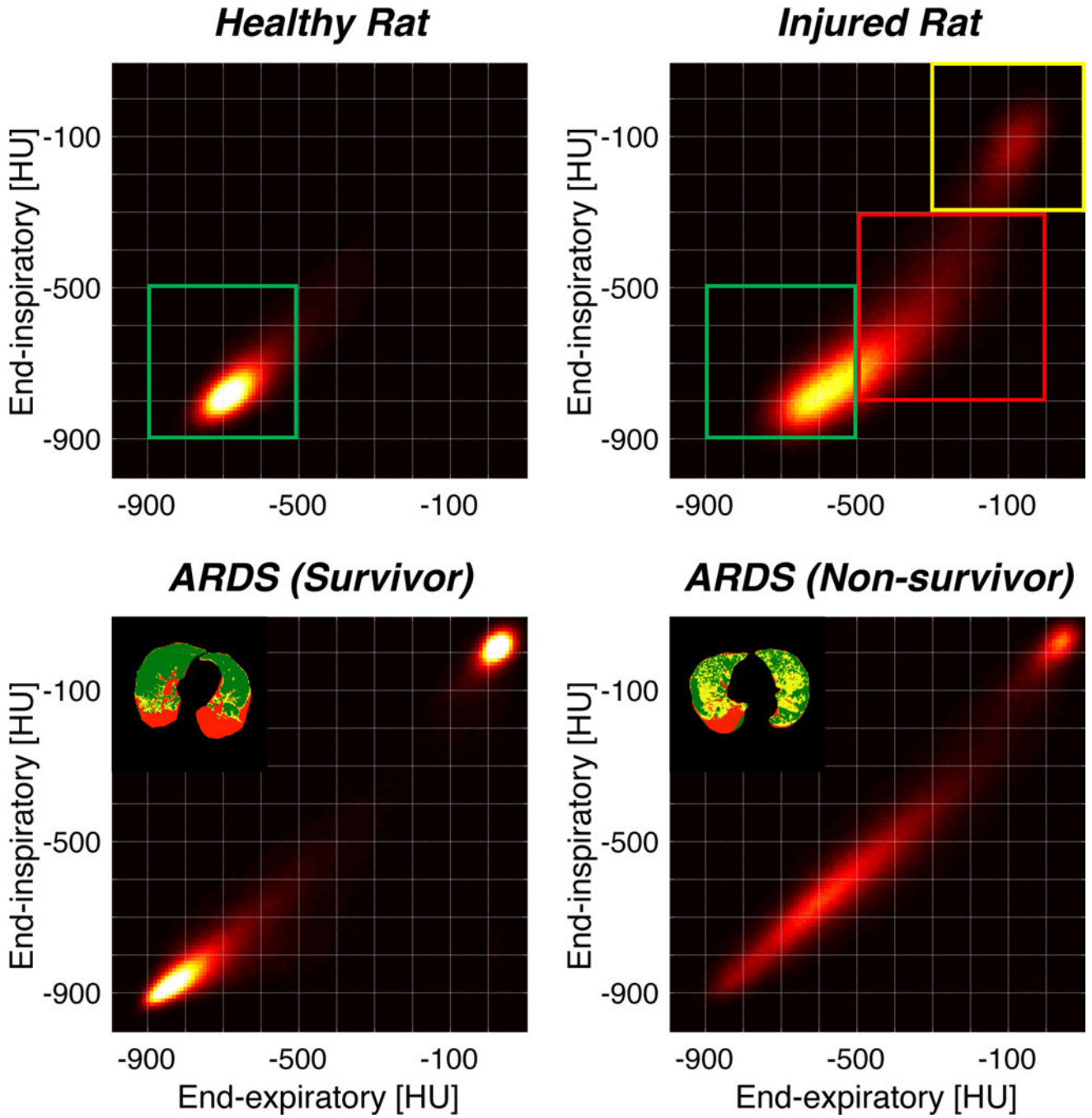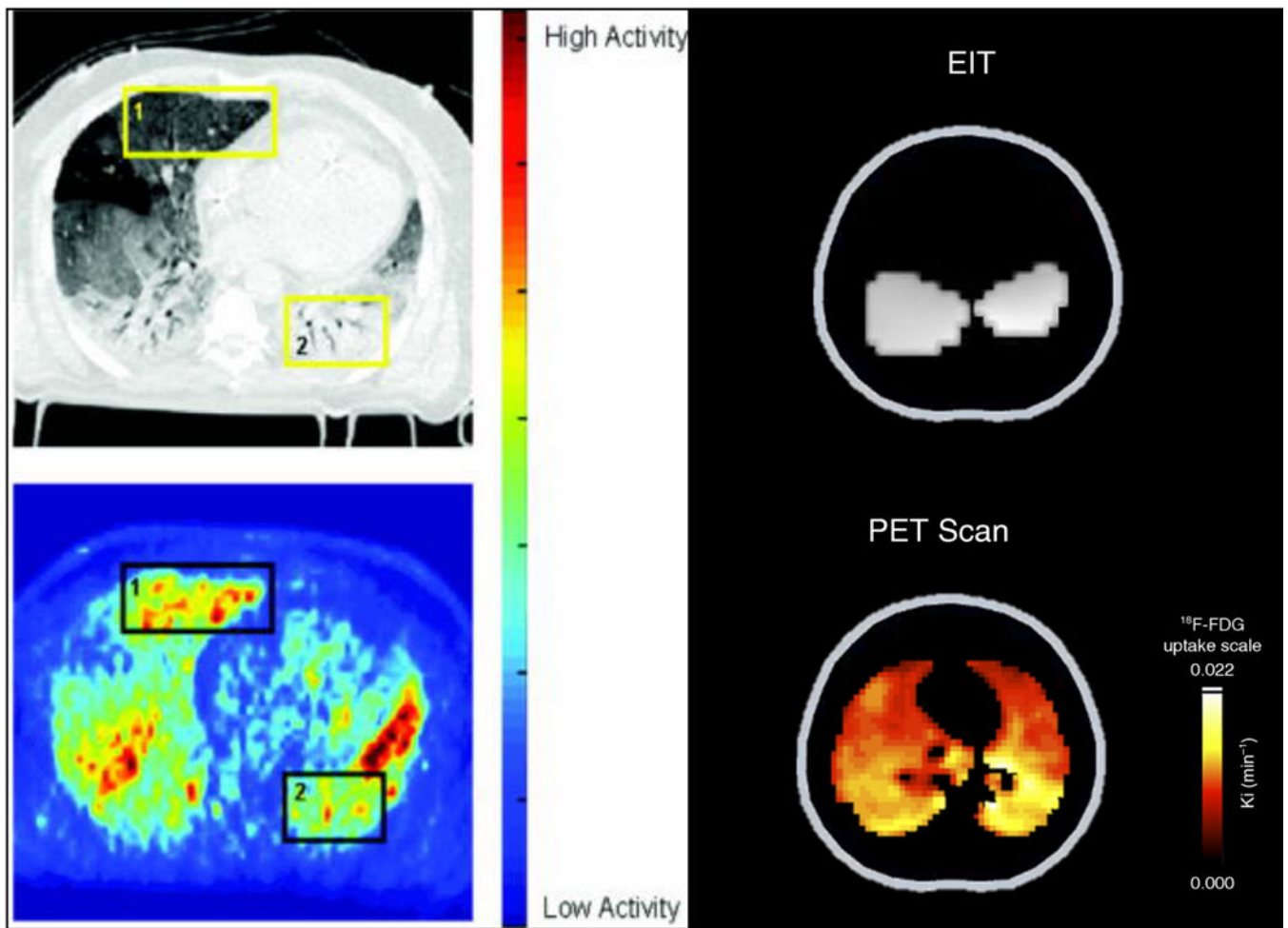
Figure 6.
Parametric response maps (PRMs) are constructed where each voxel is represented by a single point, the coordinates of which correspond to the density of the voxel (in HU) at end-expiration (X-axis) and at end-inspiration (Y-axis). In a normal rat lung (***Upper Left Panel***), almost all of the voxels (*i.e.* density of lung tissue) are clustered around -700 HU (in both axes); thus the density is uniform as expected in normal lung, and there is 'stable density', *i.e.* little overall difference in between inspiration and expiration (green box). In the injured rat lung (***Upper Right Panel***), most voxels remain within the 'normal' lung distribution

(green box). However, many voxels fall in a distribution indicating near-normal density at and-inspiration (−300 to −700 HU) and predominantly high density (minimally aerated lung; 0 to −600 HU) at end-expiration; this profile corresponds to 'unstable inflation' (red box). Finally, several voxels are clustered in the upper rightmost corner, *i.e.* high density (range of -100 HU) in end-inspiration and in end-expiration. This represents fixed consolidation (no aeration, no recruitment; yellow box). PRMs from patients with ARDS are shown (***Lower Panels***); while both patients have voxels indicating fixed atelectasis (upper right corners), the patient who survived (***Lower Left Panel***) had more voxels in the 'normal' range, and fewer voxels indicating 'unstable inflation', than the patient who did not survive (***Lower Right Panel***). Reproduced with permission Ref. 14.
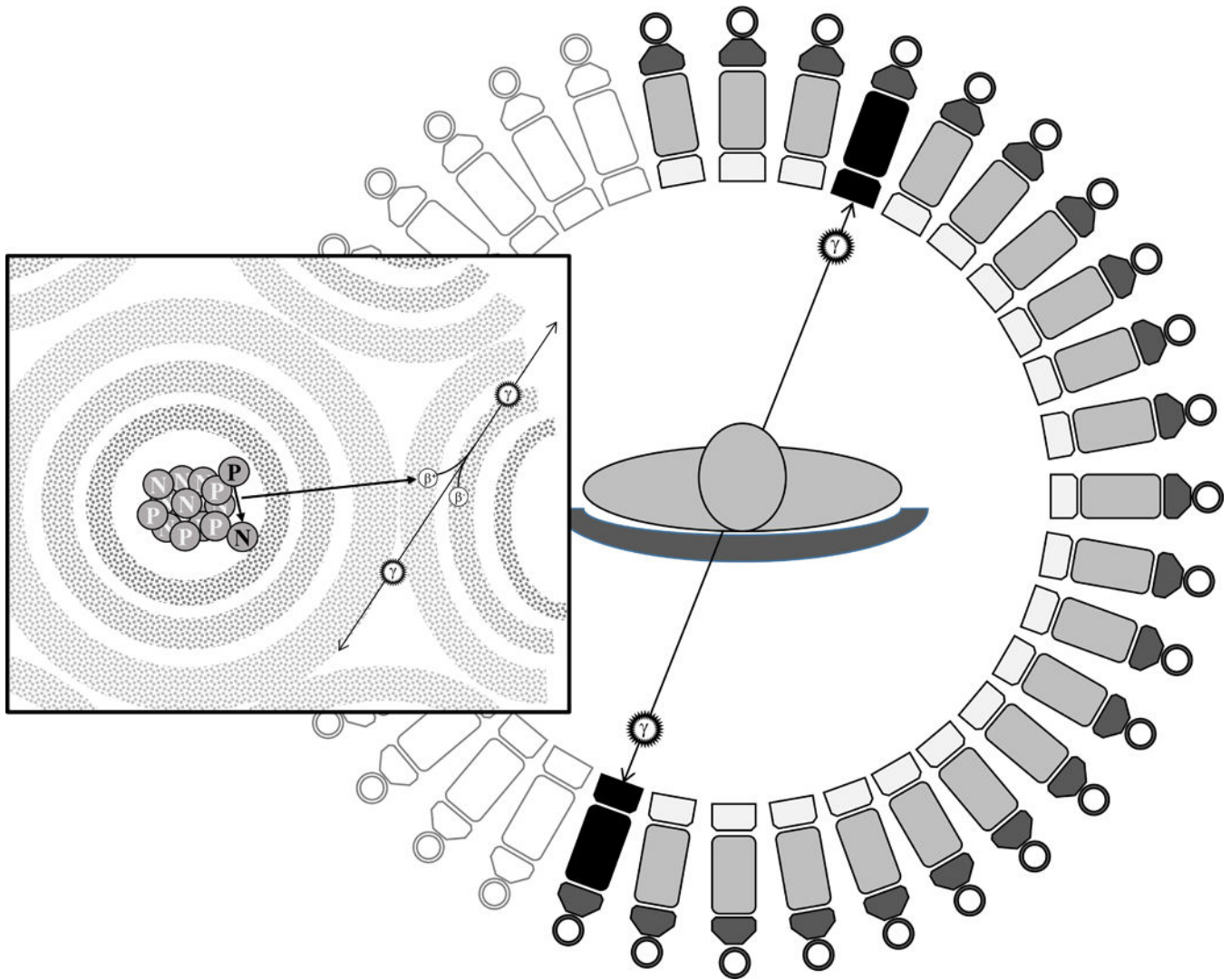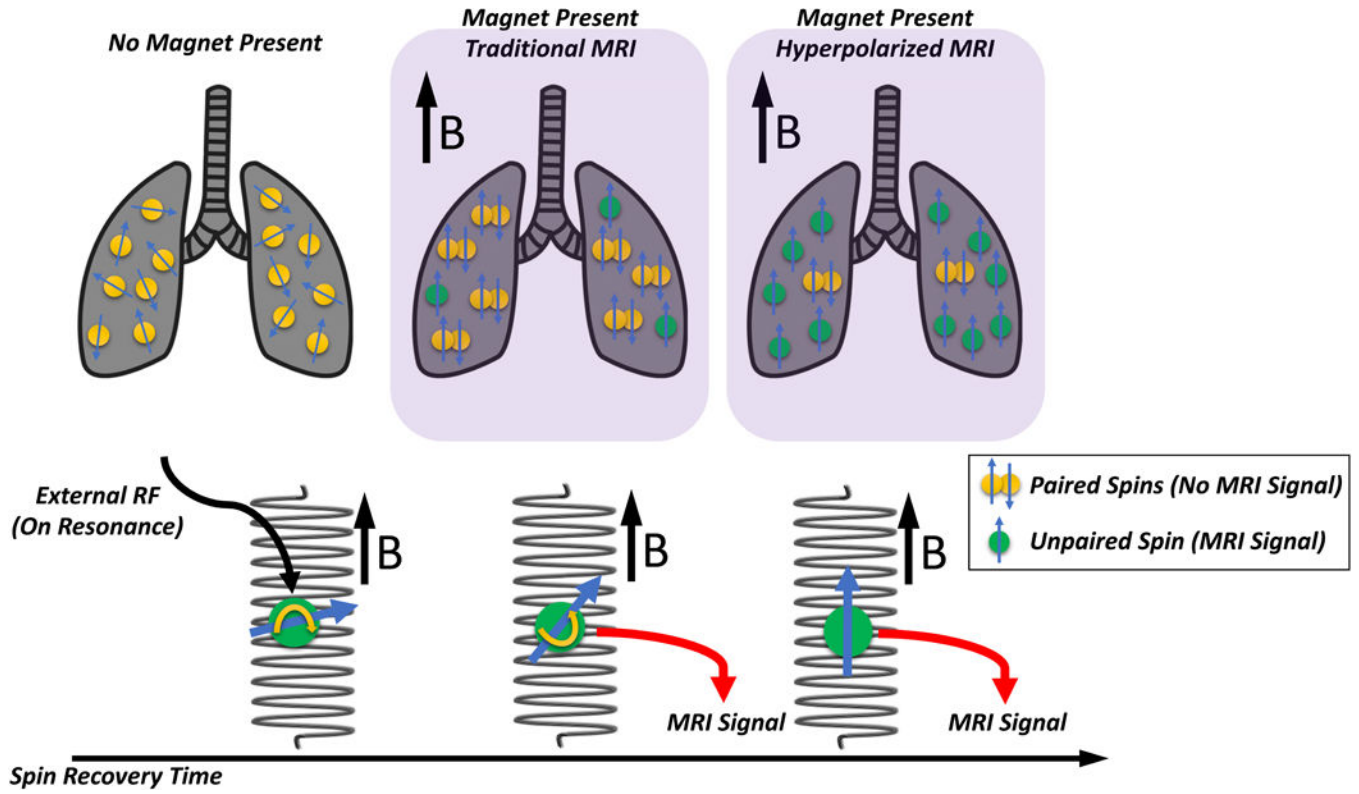
Figure 7.
Positrons (β^+) are emitted from the tracer and interact with electrons (β^-) belonging to the local tissue, causing an *annihilation* that produces two photons (Υ) travelling in opposite directions. When two photons are simultaneously sensed by the PET machine on two opposite detectors, the 'event' causing their emission is considered 'true' and their origin is plotted on the image.
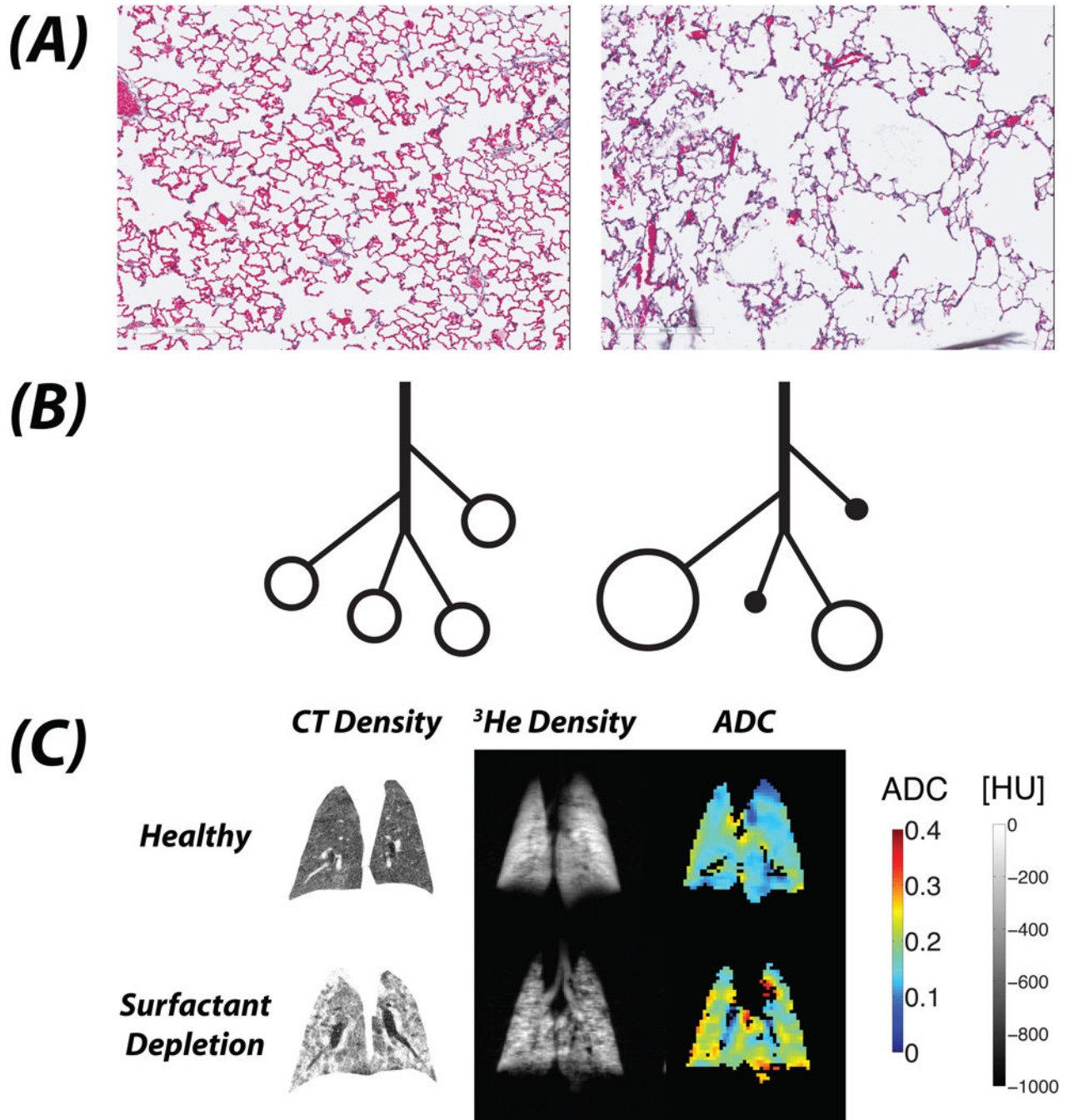
Figure 8:
Paired Computed tomography (CT, Upper Left Panel) and [18F]-fluoro-2-deoxy-d-glucose (18FDG) positron emission tomography (PET, Lower Left Panel) from a patient with ARDS. A high level of 18FDG activity is seen in the in ventral lung in the PET scan (Yellow Box 1) that appears normally aerated in the CT scan ('baby lung; Black Box 1). Paired electrical impedance tomography (EIT, Upper Right Panel) and PET (Lower Right Panel) images are shown from a pig with lung injury ventilated with low tidal volume and low PEEP, while performing strong inspiratory effort. The EIT image shows regions of maximum ventilation (grey shade) in dependent lung near the diaphragm, and the PET image shows high FDG activity, indicating inflammation, in the same dependent regions. Reproduced with permission from Refs. 168 and 170.
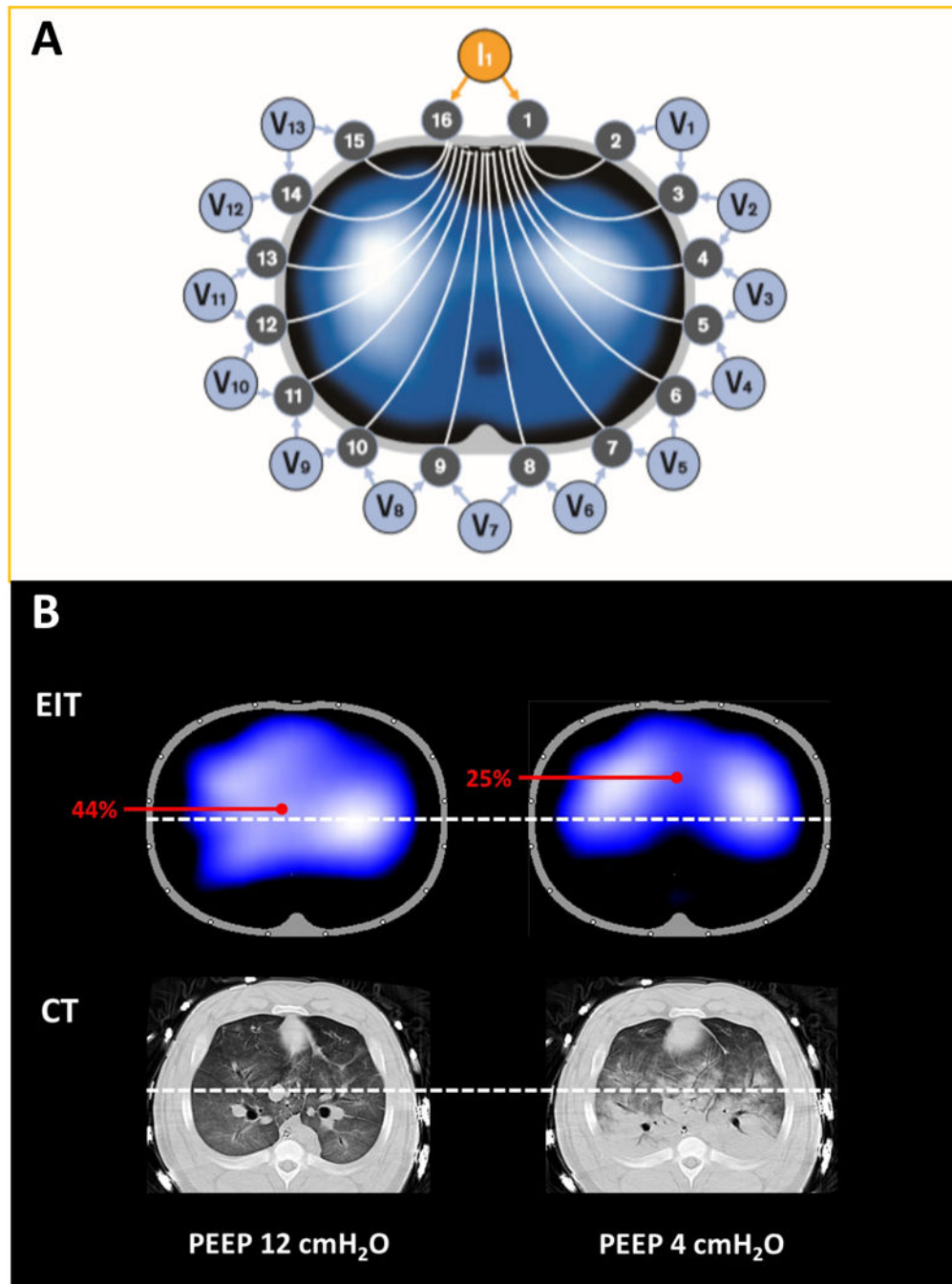
Figure 9:
Nuclear spin is an inherent property whereby nuclei spontaneously rotate; this generates the signal in magnetic resonance imaging (MRI). The schematic illustrates the impact of a magnetic field and hyperpolarization (***Upper Panels***). In the absence of a magnetic field (***Upper Left Panel***) the spins are haphazard; but, in the presence of a magnetic field (***Upper Mid Panel***), the spins are aligned with the direction of that field (or in the opposite direction: 'anti-aligned'). The direction is called the B vector. Aligned and anti-aligned spins cancel each other in pairs (paired yellow circles); but a small proportion of spins remain unpaired (green circles), and these unpaired spins generate the MRI signal. Hyperpolarization generates a far larger fraction of unpaired spins (***Upper Right Panel***) and this greatly enhances the signal. The ***Lower Panel*** illustrates the impact of an external radiofrequency energy pulse on the magnetic field. The energy pulse modifies ('flips') the axis of the spin and changes its direction, and over time the spin recovers its original orientation. However, during this recovery time, the MRI signal is collected, and because individual tissues have different recovery times, a tissue-by-tissue contrast is created by the MRI.

Figure 10:

The apparent diffusion coefficient (ADC) is a metric of the space across which a molecule can diffuse; thus in the lung, this is considered to be a correlate of the average volume of the alveolus. Compared with normal rat lung (***Panel A - Left***), the ADC is far greater in a lung with lung injury (***Panel A- Right***). When alveoli are uniformly and normally inflated, a relatively low value of ADC is recorded at end-inspiration (***Panel B - Left***). With atelectasis (***Panel B - Right***), hyperpolarized gas cannot reach non-ventilated alveoli and can only reach the ventilated units, which are hyperinflated; thus a higher value of ADC is recorded.

Coronal lung images of lung slices illustrate the differences among CT density, hyperpolarized ^{3}He Density, and ADC before (***Panel C, Upper***) and after (***Panel C, Lower***) surfactant depletion in a rat lung. The CT density is low in normal lung, and is increased following surfactant depletion where widespread atelectasis (complete - white, partial - grey) is apparent. The ^{3}He density image shows a homogeneously bright signal in normal lung reflecting uniform distribution of inhaled gas; however, after surfactant depletion, there are multiple areas of absent signal representing areas that are inaccessible to inspired gas because of complete atelectasis. The ADC maps in normal lung show mostly mid to low values (*i.e.* <0.15 cm^2·sec^{-1}); but, following surfactant depletion, areas of complete atelectasis are not visualized, whereas ventilated airspaces are easily seen and have high ADC values (*i.e.* are hyperinflated; >0.25 cm^2·sec^{-1}). This illustrates the high sensitivity of ADC to detect enlarged (*i.e.* over-distended) airspaces that appears on MRI as a homogeneous, high signal, even when surrounded by collapsed or partially deflated units; and, it contrasts to CT where the density is averaged within each voxel.

Figure 11:
Electrical impedance tomography (EIT) determines the distribution of intra-thoracic impedance (*Z*) by applying a known alternating current (*I*) to an initial pair of electrodes and measuring the resulting surface potentials (voltage, *V*) at each of the remaining 13 pairs of electrodes (***Panel A***). Next, the current is applied to the adjacent electrode pair of electrodes and the V recorded at the other electrodes; this cycle is repeated for one cycle of current applications, resulting in one set of EIT raw data expressed as inspiratory cyclic changes in impedance (Z) (Adapted from *Drager*). The cycle takes 0.02 seconds; it is repeated

continuously in each of the circuits in sequence, and the impedance is continuously measured. Because of the multiple circuits around the chest, ΔZ can be localized approximately to each of the quadrants. Because an increase in circuit impedance reflects an inspiratory increase in aeration, ΔZ reflects ventilation of the region in question. *Panel B* demonstrates the distribution of ventilation using EIT, and the corresponding aeration in CT images, in a pig with lung injury. At PEEP 12 cmH$_2$O, distribution of ventilation is homogeneous (*left upper*). The white-dots identify the mid-line bisecting the thorax. The center of ventilation (COV) is calculated as [(ΔZ in dorsal half of lung) x 100]/[ΔZ in whole lung];[187] if the mid-line is positioned, the % of ventilation that is dorsal is shown on the EIT display (and reflects COV) so that off-line calculation is not necessary. In this example (*left upper*), with PEEP 12 cmH$_2$O, COV is 44%, and the corresponding CT shows no lung collapse (*left lower*). In contrast, when the PEEP is reduced to 4 cmH$_2$O, ventilation is shifted to non-dependent lung at and COV is now 25% (*right upper*), and the corresponding CT confirmed the presence of dorsal atelectasis in the same region (*right lower*).
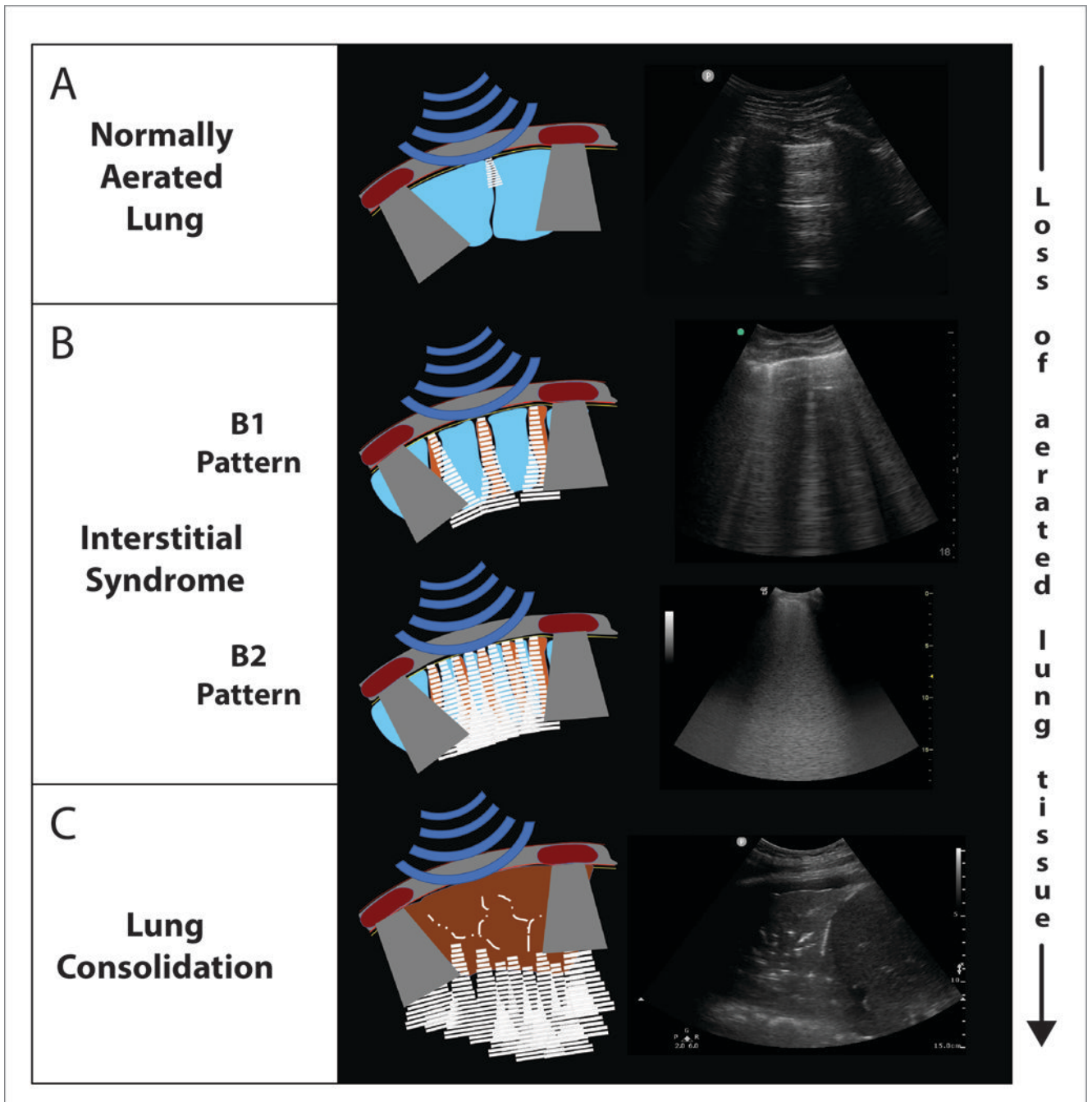
Figure 12:
Schematic and still images of lung ultrasound in normal lung (***Panel A***), interstitial syndrome (***Panel B***) and alveolar syndrome (***Panel C***). In the normally aerated lung (***Panel A***), the findings include a homogenous pleural line (uppermost horizontal white line in image), the presence of an A line (*i.e.* short horizontal white line in mid-image, an artefact from the pleural line), lung sliding (see respiratory changes seen in the dynamic video-Supplemental Digital Content 6), and a lung pulse (see cardiac changes seen in the dynamic video- Supplemental Digital Content 6). The interstitial syndrome (***Panel B***) involves loss of

lung aeration and is of two types. The 'B1' pattern, corresponding to moderate loss of aeration, has 3 or more B-lines (vertical) per intercostal space, whereas the 'B2' pattern, corresponding to more severe loss of aeration, has multiple coalescent B-lines per intercostal space. Lung consolidation (***Panel C***), indicates substantially increased density with almost complete loss of aeration. This is characterized by an anechoic (*i.e.* tissue-like) image arising from the pleural line.

Table 1.

Transducer recommendations according clinical question and findings

Diagnosis \ Transducer	Pneumothorax	Pleural Effusion	Interstitial Syndrome	Alveolar Syndrome	
				Large consolidations	Small peripheral consolidations
1st choice	High-frequency	Low-frequency (curvilinear or phased array)	Low-frequency curvilinear	Low-frequency (curvilinear or phased array)	High-frequency
2nd choice	Low-frequency curvilinear		Low-frequency phased array		
3rd choice	Low-frequency phased array		High-frequency		

Table 2.

Diagnostic accuracy of lung ultrasound for most common lung pathologies/syndromes.

Diagnosis	Alveolar-Interstitial Syndrome					Pneumothorax	Pleural Effusion	Overall accuracy
	Pneumonia	Cardiogenic Edema	Embolism	Contusion	Interstitial disease			
Sensitivity (%)	82.8–93	85.3	85–87	94.6–98	91.5	78.6	94–98	95
Specificity (%)	72–95.5	92.7	81.8–83	90–96	81.3	98.4	94–98	94
References	217–220	221	222,223	224,225	226	214	224,227	224

Legend: ARDS, Acute Respiratory Distress Syndrome; AUC, Area Under the Curve; CI, Confidence Interval